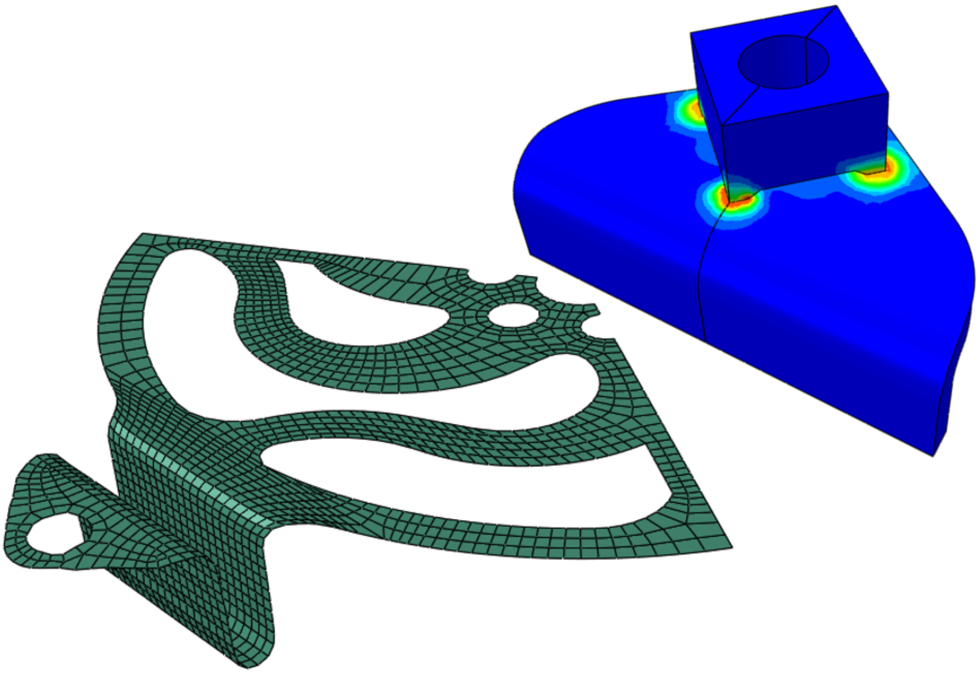

Fatigue impact of residual stresses from manufacturing processes

Master's thesis in Applied mechanics

KLAS TEGNEMYR

DEPARTMENT OF MECHANICS AND MARITIME SCIENCES

CHALMERS UNIVERSITY OF TECHNOLOGY
Gothenburg, Sweden 2022
www.chalmers.se

Master's thesis 2022

Fatigue impact of residual stresses from manufacturing processes

KLAS TEGNEMYR

Department of Mechanics and Maritime Science
Chalmers University of Technology
Gothenburg, Sweden 2022

Fatigue impact of residual stresses from manufacturing processes
KLAS TEGNEMYR

Supervisors: Kajsa Bengtsson, Azelio, Torkel Davidsson, Uniso Technologies
Examiner: Anders Ekberg, Professor at Mechanics and Maritime Sciences, Division of Dynamics

Master's Thesis 2022:44
Department of Mechanics and Maritime Science
Chalmers University of Technology
SE-412 96 Gothenburg
Telephone +46 31 772 1000

Cover: Final displacement of the flex disc and the weld nut in contact with a part of the flex disc showing a von Mises stress field.

Typeset in LaTeX
Printed by Chalmers Reproservice
Gothenburg, Sweden 2022

Fatigue impact of residual stresses from manufacturing processes
KLAS TEGNEMYR
Department of Mechanics and Maritime Science
Chalmers University of Technology

Abstract

This study was done to investigate how residual stress from different manufacturing processes could be simulated and what effect they would have on predicted fatigue life of the components.

The two manufacturing processes investigated were forming and welding. The forming process was simulated through a two-simulation process, an explicit forming simulation and an implicit springback simulation were used to evaluate the residual stress formation. There were results from the forming simulation that need further investigations to ensure trustworthy results. The welding process featured a simplified simulation divided into two parts, a heat transfer simulation and an implicit static simulation.

Results from the forming simulation gave similar stress levels as the measured values. The welding simulation did not give as good results as the forming simulation. A different method should be investigated to get more accurate results.

Residual stresses impact on the predicted fatigue life was examined by comparing a component safety factor to fatigue with and without residual stress added to the simulation. The result showed that the safety factor decreased moderately when accounting for the residual stresses due to the elevated mean stress.

This master thesis was done on behalf of Azelio in collaboration with Uniso Technologies. Azelio develops a thermal energy storage called TES.POD that uses stored thermal energy to provide energy through a Stirling engine. The system has a storage capacity of 13 hours that could work as an off-grid solar system storage.

Keywords: residual stress, simulation, forming, welding, fatigue.

Acknowledgements

First and foremost, I would like to thank Azelio and Uniso Technologies for letting me do this master thesis. I would also like to send my gratitude to my examiner Professor Anders Ekberg and my supervisors Torkel Davidsson at Uniso and Kajsa Bengtsson at Azelio who have all been supportive and engaged through the entire process. Many people at both the CAE team at Azelio and Uniso have been taking time off their days to help me throughout this thesis, I appreciate all your help. This thesis wouldn't have been possible without all the support and help I've gotten from all of you. Lastly, I would like to thank my family and my partner for all the moral support you have given me, not only through the time that I wrote this thesis but also throughout my time at Chalmers.

Klas Tegnemyr, Gothenburg, June 2022

List of Acronyms

Below is the list of acronyms that have been used throughout this thesis listed in alphabetical order:

CWM	Computational welding mechanic
HCF	High cycle fatigue
LCF	Low cycle fatigue
RSW	Resistance spot welding
TES.POD	Azelio's Thermal Energy Storage
TWI	The Welding Institute

Nomenclature

Below is the nomenclature of parameters that have been used throughout this thesis.

Parameters

α	Friction coefficient
σ_y	Yield stress
σ_u	Ultimate strength
$\sigma_{red,fl}$	Reduced fatigue limit
$\sigma_{red,flp}$	Reduced fatigue limit pulsating

Contents

List of Figures

List of Tables

1
Introduction

The following chapter will describe background and aim of the project. It will cover the parts that will be the foundation of the simulation models, and outline which impact this project will have on society.

1.1 Background

This master thesis will be on behalf of Azelio in collaboration with Uniso Technologies.

Azelio is a Swedish company with a Stirling-based system with thermal energy storage for dispatchable electricity production. The system has a storage capacity of 13 hours production at nominal power. The initial target market is between 0.5 – 20 MW expanding into 100 kW to 100 MW, a segment that lacks cost-effective and sustainable alternatives. Azelio's solution could for example work as a microgrid system as load shift, distributed sustainable baseload, or work as an off-grid solar system with storage.

Azelio wants to optimize the production of Azelio's Thermal Energy Storage (TES. POD) and parts for their Stirling engine. They are in the need of an investigation on how much impact different manufacturing methods have on the product, in terms of residual stresses effect on strength margins and service lives.

Azelio's TES.POD uses an aluminium alloy that is heated up to almost 600°C. When power is required, heat is transferred to a Stirling engine through a heat transfer fluid. The Stirling engine can then provide 13 hours of electricity at continuous operating power. This process includes thermal cyclic loads and mechanical loads from the engine.

1.2 Aim

The main objective of this master thesis will be to make a literature study on how residual stresses in manufacturing processes, e.g. welding and forming, should be calculated and handled. If there would be a need for a post-process treatment, which would be suitable for the different types of manufacturing processes? This will also include comparing different simulation software on the market to see how they handle residual stresses.

The literature study will then be used to analyze the life of a given component in the TES.POD. It will include constructing the FE-based simulation model and analysing the response of thermal and mechanical loads. The resulting residual stress will then be compared with results from physical tests of residual stresses after manufacturing the component. These results from test data already exist. Additional tests will only be conducted if the given test data need to be complemented.

1.3 Limitations

Manufacturing processes that will be considered in the literature study are welding and bending. The resulting theory from the literature study will be applied to the analysis of two selected parts of the TES.POD and not the entire product. To select which software to use, a search of what is used in the industry and current research will be conducted. Two codes will then be compared more in-depth. The main objective of the thesis will be to analyse the residual stresses after manufacturing. This data will then be considered when calculating the fatigue life of the test part. Fatigue analysis will only be conducted on parts that are exposed to cyclic loading.

1.4 Research questions

The following questions are planned to be answered during the project.

- How can residual stresses be calculated for welding and forming?
- What can be done to make the residual stress distribution more benign?
- How well does theoretical results compare to physical test results?
- How are different computational software calculating residual stresses?
- How do the residual stresses affect the predicted fatigue life predictions?

1.5 Specific components under investigation

The following subsections present the two parts that will be evaluated during the project. The two parts are denoted "bowl" and "flex disc". The exact dimensions of the parts are not given in this report.

1.5.1 Bowl

The bowl can be seen in Figure 1.1. It is cold-pressed from cold-rolled 3 mm sheets of stainless steel. Measurements of the residual stresses are made in the centre and at the five marked points as indicated on the outer surface of the bowl in Figure 1.1. The stress is measured in the radial and tangential directions.

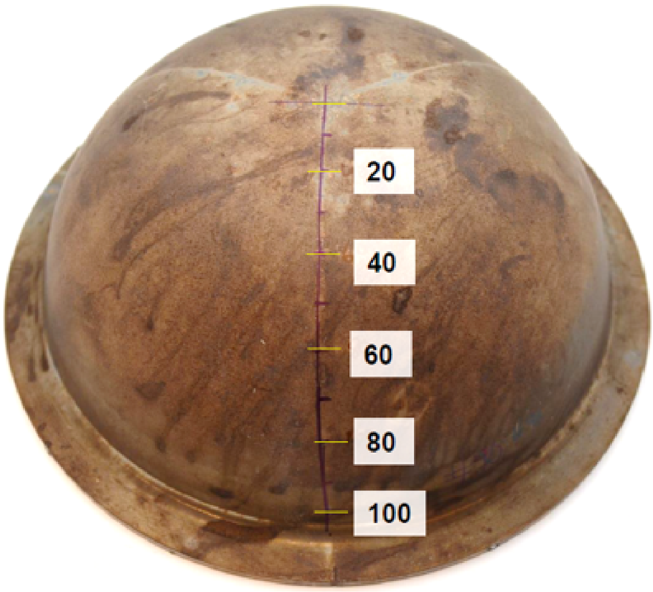

Figure 1.1: The bowl with positions for the measurement points in mm from the center.

1.5.2 Flex disc

The flex disc is displayed in Figure 1.2. It is made from a 3 mm steel sheet. Manufacturing techniques used are laser cutting the shape, bending the fasteners, one 180-degree bend and two 90-degree bends, and then resistance spot weld the nuts. Residual stress has been measured at the three places marked in Figure 1.2, where the part has been bent. In addition, there are three measurements taken right underneath the nuts (denoted weld profile), along the curvature of the bend, see Figure 1.3. Three measurements are also taken approximately 10 mm to the left of these measurements(denoted radius profile), as seen in Figure 1.3. The measurements made on the 180-degree bend are taken in 6 places along the curvature of the bend, see Figure 1.4 and Figure 1.5. For all cases the residual stress has been measured in two directions: along the curvature and 90-degrees off from the curvature direction. In the Figure 1.3 and Figure 1.5 these directions can be seen as radial and tangent direction respectively.

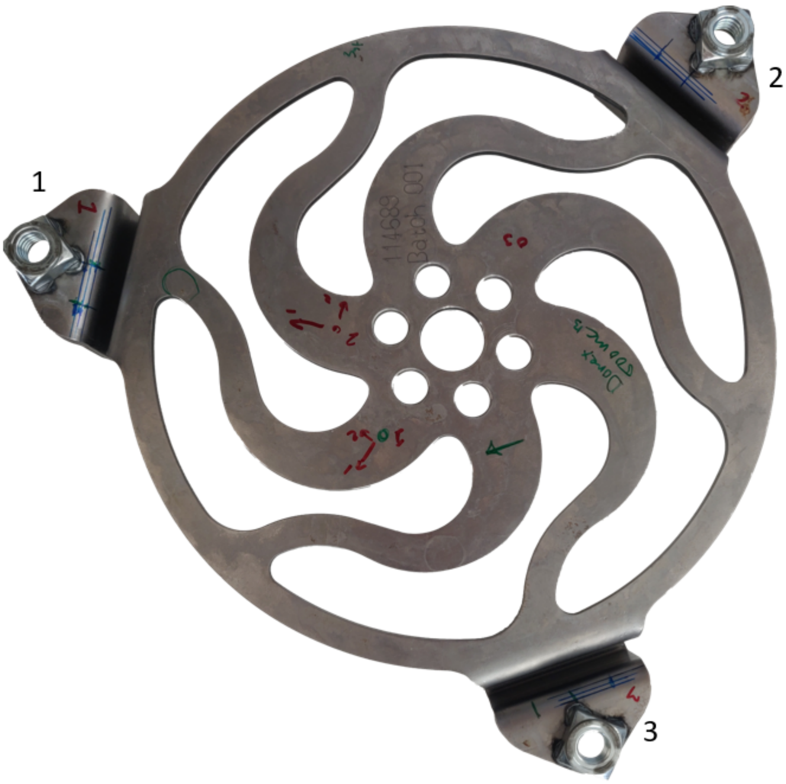

Figure 1.2: The flex disc showing the three fasteners where the measurements was made.

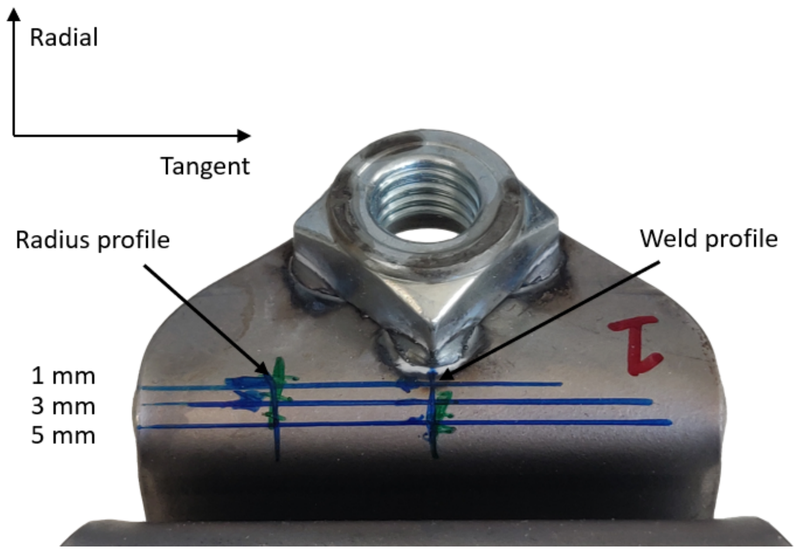

Figure 1.3: The 90-degree bend of the flex disc at position 1 in Figure 1.2. Distances presented on the left are measured distances from the weld toe.

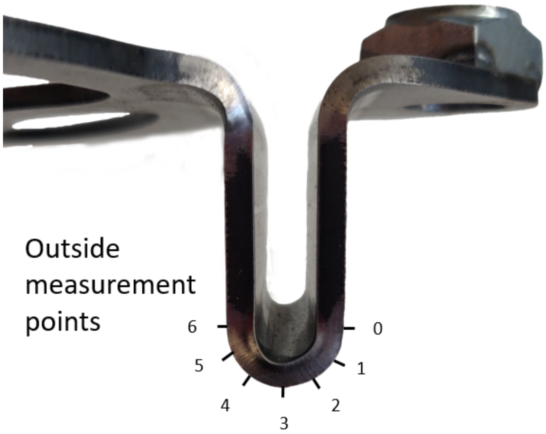

Figure 1.4: The 180-degree bend of the flex disc in position 1 in Figure 1.2. Positions 0–6 represents the measurement points.

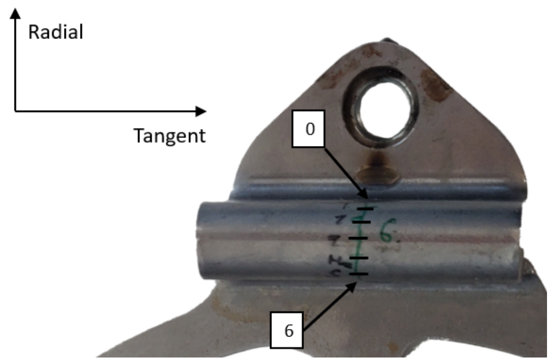

Figure 1.5: The 180-degree displayed from underneath. The two directions in which the measurements are made are shown as radial and tangent. Distance between the points are 3 mm.

1.6 Societal impact

This project was started to improve the assessment to ensure that the product would hold for multiple load cycles with a proper safety factor. In that aspect, the ethics of the project will be to ensure a better product which will benefit the customers of the product, and better use of material since tolerances can be better estimated. If the product is in use for a longer time it generates a positive influence ecologically.

2
Theory

Theoretical aspects of the project will be discussed. This includes a description of residual stresses, why they occur, how to measure and how to predict them. Computational welding mechanics, material models, and fatigue are also described.

2.1 Residual stress

Residual stress is the stress that remains in the material after the stress magnitude in parts of an object has exceeded the yield limit and plasticized and then been unloaded. This can occur due to different procedures. Mechanical processing that is not uniform through the entire part such as bending or extruding may cause residual stresses. Thermal variations, e.g. welding, can also create residual stresses in an object. High temperatures are distributed around the area of the weld in the object resulting in restricted expansion. When temperatures are cooled down the cooling rate is different throughout the object. The different cooling rates will generate differences in thermal contractions which will lead to non-uniform stresses in the object that may promote the formation of residual stresses.

Detecting residual stresses can be done through different methods. These methods can be divided into three categories: non-destructive, semi-destructive and destructive. Non-destructive methods include for example X-ray diffraction and neutron diffraction, these measure the crystal lattice spacing in an object, which can be used to determine the residual stresses. Semi-destructive methods imply taking away a small amount of material to calculate the residual stresses. Examples of such methods are centre hole drilling and deep hole drilling. Both these methods are different ways of drilling holes into the object and then measuring the deformation at the hole after redistribution of the residual stresses. Destructive methods are destroying the integrity of the object. An example of such a method is slitting which is, in a similar way to the semi-destructive methods, measuring the deformation after redistribution of the residual stresses by cutting a slit through the entire object. These kinds of destructive methods are often used in research and development.

There are different ways to alter the residual stress field in an object. Post-processing procedures such as shot peening and cold rolling can be used to redistribute the residual stress in an object. Heat treatment can also be used to reduce the residual stresses. It can also be of interest to look at the welding technique. If it is possible to weld at a lower temperature, for a shorter amount of time, then the heat transferred into the object would be less which would result in less residual stress. Procedures such as longer cooling time and preheating the object can also be used to reduce residual stresses. For a more thorough description of the methods mentioned check The Welding Institute (TWI) website regarding residual stress [1].

To calculate the residual stress a specific manufacturing technique would generate, finite element simulations can be used. This will include complex non-linear analyses where assumptions and approximations, e.g. regarding material behaviour, will be needed. When simulating welds, aspects such as temperature, time and welding setup must be considered. These are often hard to determine and approximations are often required.

2.2 Computational welding mechanics

Computational welding mechanics (CWM) will include material and thermal components which are affected over time which results in a challenging simulation procedure. Zacharia et al. [2] divided the procedure into modelling four phenomena: heat and fluid flow, heat source–metal interaction, weld solidification microstructure, and plastic transformations. These are described in detail in [2].

The welding technique used on the flex disc was resistance spot welding (RSW). It uses an electrical current through the parts that are going to be fused. The resistance between them heats the materials. This with a combination of an applied compressing force welds the parts together. Electrical, thermal and mechanical aspects need to be considered which makes a complex simulation process. Further discussions on how to simulate RSW can be seen in chapter 3.

2.3 Material models

The purpose of material models is to characterise the stress–strain response of a material in numerical simulations. For a material such as steel, two parts need to be considered: the elastic and the plastic deformation. There are different ways to simulate these two. One straightforward model is the linear elastic perfectly plastic model. This model follows linear elasticity, Hooke's law, until yield stress is reached where the plastic deformations will increase while the stress stays at yield stress. This model is very simplified and is not taking the non-linear properties of the plastic deformation nor viscoelastic and viscoplastic properties into account. Other models deal with these issues, but it comes with the cost of more material parameters and non-linear equations. For specific methods and how to calculate them see Saabye Ottosen and Ristinmaa [4]

2.4 Fatigue life predictions

Fatigue in a strength theory perspective is due to repeated or cyclic loading of a material. Failures related to fatigue start with cracks that grow for every repeated loading until they reach a critical length which leads to failure of the component. Cyclic loads will open and close the cracks and for every opening, the crack grows. Therefore, cyclic loads in tension are more critical than in compression. The cracks can be initiated by defects in the material that create stress concentrations in the material. These defects can be on the grain level, at the material surface. They are more detrimental in poorly manufactured parts, e.g. welds with sharp edges, transitions with small radii or high residual stresses. The initiation of cracks often occurs at the surface of the material. There are however examples of crack initiation under the surface, e.g. due to rolling contact. Failure of the material can occur at lower stress magnitudes for cyclic loading than for static loading.

If the load is such that plastic deformation will occur at each repeated load, then the material will not last for as many cycles as if the repeated load magnitude would stay within the elastic range. These two load cases are referred to as low cycle fatigue (LCF) or high cycle fatigue (HCF) respectively. The number of cycles that HCF versus LFC represents is vague. According to Dowling et al.[5], HCF is in the millions of cycles and LCF is in tens, hundreds or thousands.

In fatigue life predictions an important value is the fatigue limit. This is the stress magnitude below which, an infinite number of load cycles can be sustained without causing fatigue failure. The fatigue limit is the limit of a Wöhler curve (also known as an SN curve) which describes the fatigue life in number of cycles as function of stress magnitude. With known stress levels this curve can be used to predict the fatigue life. If the stress levels are below the fatigue limit the safety factor for fatigue can be calculated with a Haigh diagram. A Haigh diagram uses the fatigue limit, pulsating fatigue limit, yield stress and ultimate strength of the material to set the boundaries for fatigue. Then the stress amplitude and mean stress for the critical positions are used to calculate the safety factor.

3
Simulation study

The following chapter will describe the approach by which the different simulation software were tested. It will cover the employed method and on which software it will be performed.

3.1 Forming

To estimate the residual stress after the bending procedure the manufacturing process needs to be simulated. First the bending and then the unloading, which will give a springback effect. The result of this procedure, with well-represented material parameters and material model, will give the residual stresses in the component. There are different studies done on how to simulate the springback effect which are mentioned later in this section.

Large, three-dimensional, non-linear deformations during manufacturing simulations can get convergence problems with an implicit solver. A reason for this, according to Sun et al.[6], can be that as the reduction of the time increment continues, the computational cost in the tangent stiffness matrix is increased and causes divergence. It is also mentioned that local instabilities cause force equilibrium to be difficult to achieve.

To overcome the disadvantages of an implicit solver, an explicit solver can be implemented. According to Prior [7], some advantages of using an explicit solver are that it is robust in analysing contact problems and calculation time is not increasing with the size of the model in the way that it is with an implicit solver. The downside of solving explicit is that the time step must be smaller than a critical value that is based on the highest eigenvalue of the part. The reason for this is that an explicit method is conditionally stable. In metal forming this can become problematic due to that the critical time often is small in comparison to the time of the forming process. To overcome this, methods such as load factoring and mass scaling can be implemented [7].

To perform the forming analysis consisting of loading and the unloading, both implicit and explicit methods can be used. For large, non-linear deformations, however, an explicit method is advantageous. The problem with performing the entire forming analysis explicit is that the unloading will result in a free vibration of the part which will continue indefinitely [7]. Two solutions to this problem are to implement some damping to the part, or transfer the explicit results to an implicit solver and carry out the springback analysis. The latter solution has been carried out by both Narasimhan et al. [8] and Yetna n'jock et al. [9] where ANSYS with LS-DYNA and ABAQUS have been used respectively. For a better understanding of the differences between implicit and explicit see the article by Yang et al. [10].

The resulting residual stress in cold-formed steel members has been analysed by Weng et al.[11]. The results from this paper can be compared with the resulting stress from the simulations in regards to the direction of the stress after the spring-back.

3.1.1 Bending test assembly

To be able to make a comparison between the different FE-calculation software, a simple assembly to simulate the bending was created. The measurements of the parts in the bending test were made to represent the 90-degree bend of the flex disc. It was done by first creating a three-part model in CATIA consisting of a die, punch and plate. The drawings of these parts can be found in Appendix A.1. These three parts were then assembled and saved into one step file that could be opened in different calculation software. The assembled three-part model can be seen in Figure 3.1.

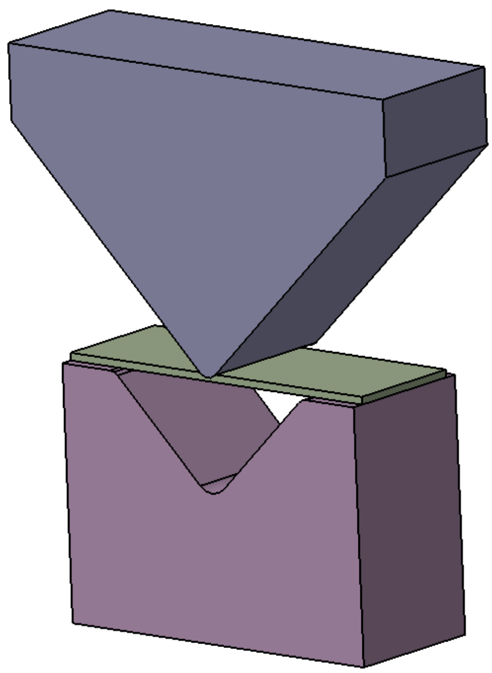

Figure 3.1: Assembly of parts to test bending simulation.

3.1.2 Bending simulation

This section describes how tests of the two chosen simulation software were done for the bending simulation. The chosen simulation software to make tests in was Ansys and Abaqus. This decision was based on two main reasons. Firstly, during the literature study, Anasys and Abaqus were the most frequently mentioned simulation software. The second reason was the accessibility, hence both Ansys and Abaqus were available through Chalmers. This made the comparisons straightforward without the need of using limited student test versions. The simulation framework describes what has been done in both software. Final simulations are presented in the two last subsections.

3.1.2.1 Simulation framework

Different methods of simulating the bending procedure were tested. A two-dimensional model of the bending test described previously, was implemented. This was done to shorten the simulation time. The material model used for these tests was Stainless-steel non-linear which was predefined in Ansys. Same material model was implemented in Abaqus. The die and punch were set to be rigid bodies. First, an implicit solver was used. The bending was displacement driven and despite the number of time steps, convergence was not achieved in any of the software. For the explicit solver, a velocity and a time were set. With the explicit solver, the entire 90-degree bend was achieved in both Abaqus/Explicit and Ansys Explicit dynamics. For the full three-dimensional bending model hexahedron elements were first implemented. This resulted in a time-consuming simulation and difficulties with hourglass effects. For the second attempt, a mid-surface shell model was applied. This drastically lowered the simulation time and gave promising stress results in form of magnitudes and directions, in both the software. To simulate the springback effect, the stress field and the displacements were mapped on the plate in an implicit solver as an initial state. The implicit solver then calculated the springback which resulted in the final stress field. The final simulations in Ansys and Abaqus are presented in detail in the following subsections.

3.1.2.2 Ansys

The explicit solver in Ansys Workbench was Explicit dynamics which uses AUTODYN. Narasimhan et al. [8] uses LS-DYNA as an explicit solver which was not possible for this project due to a lack of licences. Mesh size was set to 3 mm for the plate with three integration points through the thickness. The body interactions parameter was applied as a friction coefficient α= 0.15 which was an estimated value. The die was set to be a fixed support, the punch was given a velocity of 0.25 m/s and the boundary condition to move only vertically. The middle part of the plate under the punch, was given the boundary conditions to only move vertically. The simulation ended when the punch had moved the defined distance to perform the 90-degree bend.

Six stress results for each of the three integration points and the position of the nodes were exported to a text file. These results were then imported into Workbench as External data. This had to be done since the results from the Explicit dynamics could not be transferred to the implicit solver Static structural directly. Engineering data, Solution and External data were coupled with Static structural. The Solution coupling transferred the 90-degree bend geometry of the plate to Static structural. In Static structural, the imported stress field was mapped onto the deformed geometry of the plate in the three integration points as an initial stress state. Fixed boundary conditions were applied to one of the short sides of the plate.

The results of this method were not successful. With multiple attempts to map the stress field onto the plate, the initial stress field of the Static structural did not match the final stress field of the Explicit dynamics. The anticipated springback effect did occur but the stresses did not change in a manner similar to what was found in Weng et al. [11] and the measured test results.

3.1.2.3 Abaqus

The explicit solver in Abaqus was Abaqus/Explicit. Mesh size was set to 3 mm with five Gauss points through the thickness. A material model that resembled the Stainless-steel NL from Ansys was applied. An estimated friction coefficient $\alpha=$ 0.15 was implemented in the contact between the die and plate and the punch and plate. The die was set to be a fixed support, the punch could only move vertically with a downwards velocity of 0.25 m/s, and the plate was fixed in the horizontal direction along the length of the plate. Time was applied to the setup to set how far the punch would move.

The result from the explicit solver was then set as an initial state in the implicit solver in Abaqus/Standard. This was done by inserting only the plate in Abaqus/-Standard, mapping the stress field in an initial state, and putting a fixed boundary condition on one of the short sides of the plate.

Results from the implicit analysis were of the same character as the results presented by Weng et al. [11]. The outside of the bend had compressive stress along the bend and the inside had tensile stress along the bend. When comparing this with the test results, the stresses are of the same magnitude.

3.2 Material models

To simulate the manufacturing process of the bowl and the flex disc, three material models need to be created. These models need temperature-dependent parameters. The material properties of the bowl are well defined. Material properties for the weld nut and flex disc are not as well defined. Hence, for this project, the thermal material properties will be approximated. Josefson et al. [14] present a simplified FEA simulation of a welding procedure. The paper presents thermal and mechanical properties for S355. The composition of S355 is close to the composition of the material in flex disc and weld nut. Therefore, the thermal behaviour, presented in the paper by Josefson et al. for S355, will be implemented in the material models for the flex disc and the weld nut. One difference between S355 and the material used in the flex disc and weld nut is the yield stress at 20^{o}C. In this project, the temperature-dependent yield stress will be assumed to follow the reduction presented by Josefson et al.[14]. By applying the same percentage reduction for each temperature change, similar temperature-dependent yield stress can be estimated for materials with different yield stress at 20^{o}C. Because of the lack of material data, a bilinear isotropic hardening model will be applied. The hardening model will be based on the yield stress and the ultimate stress. It will be assumed that the ultimate stress occurs at approximately half of the fracture elongation A_5. This assumption is based on a tensile test made on the material in the flex disc at 20^{o}C.

Appendix A.3 to A.5 display the material parameters implemented in the numerical models for the bowl, flex disc and weld nut respectively. The same density, 7850 kg/m^3, was applied to all three material models. Fracture elongation A_5 for the materials was approximately 30% for the flex disc and 40% for the bowl. The weld nut was assumed to have the same fracture elongation as the flex disc. Linear approximations are made between the numerical parameters in the material models.

3.3 Resistance spot welding

Resistance spot welding (RSW) is a welding method that uses heat created when a current passes through two resistive materials. The heat melts parts of the material in contact and welds them together. Three aspects need to be considered when simulating RSW: electrical, thermal and mechanical. To consider all three aspects, a well-defined material model is necessary. Zhang et al.[12] mention that an ideal and realistic model simulation of RSW processes should include a thorough heat transfer analysis, electrical field analysis, thermo–elastic–plastic analysis, actual variation of contact resistance, phase change, and temperature-dependent material properties. These material and contact properties require extensive testing which is not always available. Therefore, approximations need to be implemented.

Zhang et al.[12] describe a method where a coupled electrical-thermal-mechanical analysis can be implemented to analyse RSW. Such a method was performed by Nielsen et al.[13]

Nielsen et al.[13] use an electro-thermo-mechanical FEM implementation in the software SORPAS 3D, which is designed to calculate complex RSW simulations. The method is integrating the mechanical, electrical and thermal modules for every time step. This method requires small time steps to capture the effects of the welding procedure. The article compares FEM simulation results to physical experiments where the cross-section of the weld was visually examined to compare the shape and thermal impacts. Different currents, contact criteria and weld time were investigated.

3.3.1 Weld nut test assembly

To compare the welding process in different software, a quarter of a weld nut in contact with a plate was created. A two-part model was created in SpaceClaim and the measurements of the model can be seen in appendix A.2. The height of the fuse part of the weld nut was modelled to be in between the original and final height. Original height of the fuse part was 1.2 mm and the final height was 0.5 mm, and the modelled part was 0.9 mm. This was done to simulate a mid-state of the welding process. The model was saved as a step file which could be imported into different software. Figure 3.2 displays the assembled model.

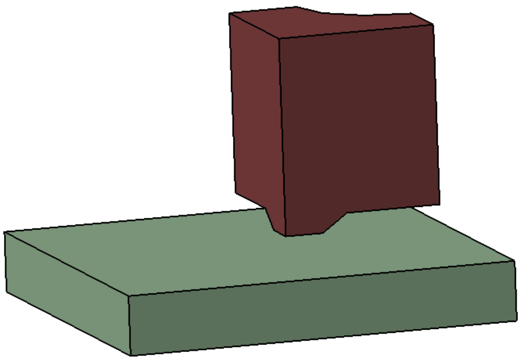

Figure 3.2: Assembly of parts to test weld nut simulation.

3.3.2 Weld nut simulation test

This section describes how tests in Ansys and Abaqus were done for the resistance spot welding. The simulation framework describes what has been done in both software. The last simulations in the two software are presented in the two final subsections.

3.3.2.1 Simulation framework

To simulate the resistance spot welding process, the electro-thermo-mechanical iterative procedure was investigated. Abaqus has coupled thermal-electrical-structural solver and Ansys has a coupled thermal-electrical solver. These two coupled solvers need complex contact and material criteria which were out of the scope for this project. Therefore, ways of simulating this without using electrical parameters were looked at.

Nielsen et al. [13] present the temperature in the welding process in their article. This shows that there is a small region around the contact area that reaches above melting temperatures. This was used to approximately simulate the heating procedure of the welding process. The contact surface was ramped from room temperature to the melting point in the same amount of time as the welding procedure and was then cooled down to room temperature. This created a temperature change in the model that was imported in a structural analysis which simulated the deformation and stress field created by the heat. The material models described earlier for the plate and the weld nut was used for this test.

Resulting stresses from this thermal and structural analysis shows similarities with the results from the physical test data. The stresses around the weld had the appearance as the test results. Consequently, this method was chosen to be used for this project. The final simulations in Ansys and Abaqus are presented in detail in the following subsections.

3.3.2.2 Ansys

The thermal analysis was performed in Ansys Workbench with a transient thermal analysis. Mesh size was set to 1 mm with hexahedron elements. A bonded contact condition was applied between the nut and the plate. In the contact surface between the weld nut and the plate, a ramped temperature was applied from 20 ^{o}C to 1520 ^{o}C for 150 ms. The simulation then ran until the temperature of the entire assembly was less than 40 ^{o}C. The solution from this simulation was then used as the setup for a static structural analysis.

For the static structural analysis symmetry boundary conditions were applied on the weld nut as well as on the edges of the plate beneath the weld nut. The bottom part of the plate was locked in the vertical direction but was allowed to move in the horizontal direction without friction. A force of 875 N was applied on the top of the weld nut for the first 150 ms. The force was then released for the cooling process.

This solution worked well when Young's modulus and Poisson's ratio were not time-dependent. For time-dependent Young's modulus and Poisson's ratio, however, convergence issues appeared in the static structural analysis.

3.3.2.3 Abaqus

Thermal analysis in Abaqus was made with two transient heat transfer steps, heating and cooling. Mesh size was set to 1 mm with hexahedron heat transfer elements. The thermal conductance condition in the contact between the weld nut and the plate was set to $1{\cdot}10^{10}$ W/m$^2{\cdot}$C for full contact. This was done to simulate equal heating on both sides of the contact with close to non-resistance of the heat flux. A ramped temperature was applied on the contact surface from 20 ^{o}C to 1520 ^{o}C for the heating step. This step was set to 150 ms, the length of the welding time. The cooling step was simulating cooling from the heating step until the entire assembly was less than 40 ^{o}C.

The resulting heat field was then imported into the static analysis as a predefined field. Mesh size was kept the same, but the elements were changed to hexahedron 3D stress elements. Symmetry boundary conditions were applied on the weld nut as well as the edges of the plate beneath the weld nut. The bottom part of the plate was locked in the vertical direction but was allowed to move in the horizontal direction without friction. Pressure was applied on the top of the weld nut representing the 875 N that were acting on the nut during the first 150 ms. Interaction properties in the contact were set to a rough friction formulation and hard normal behaviour with no separation allowed after contact.

Results from the simulation resemble the results from the physical tests. The stress in the plate has a similar magnitude to the measured spots.

3.4 Conclusion

The software that will be used in the project will be Abaqus. This decision was mainly based on the coupling between explicit and implicit. There are probably ways to get the mapping to work as intended in Ansys, but due to the uncomplicated mapping, Abaqus was advantageous. Another advantage with Abaqus was that there were no convergence issues when using time-dependent material models. These issues, that occurred in Ansys may also be possible to solve but since they did not appear in Abaqus it strengthened the choice of the solver.

4

Bowl simulations

In the following chapter, the simulation of the bowl is presented. It describes the method used, the result, and a discussion.

4.1 Method

To model the pressing parts to simulate the manufacturing of the bowl, the CAD part of the bowl was used. The inside of the bowl was used to create the punch and the outside was used to create the die. To keep the plate in place during the pressing process, a holder was created. Since the bowl was symmetrical an axisymmetric analysis was applied. Therefore, the manufacturing parts were made as rigid lines. The plate was made as a rectangle with a thickness of 3 mm and a length to cover the pressing procedure. Figure 4.1 displays the assembly of the manufacturing simulation.

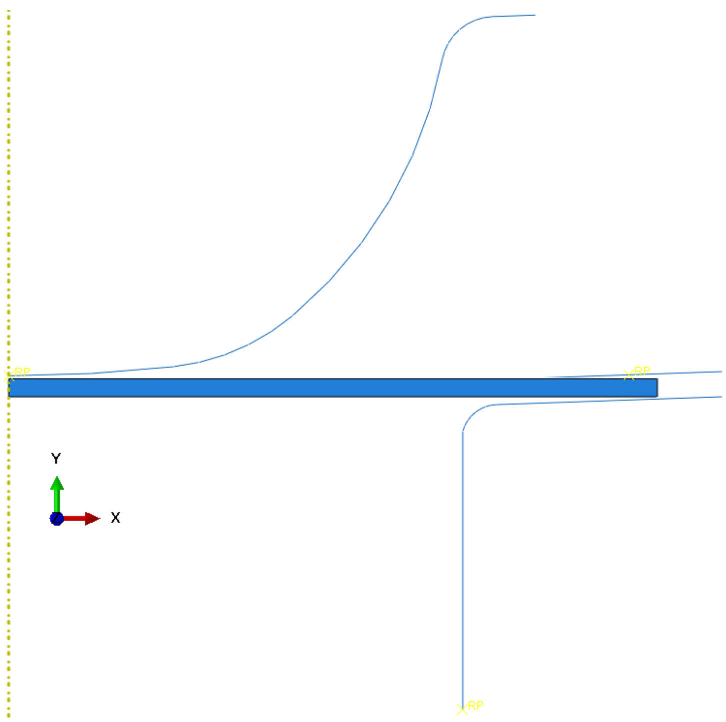

Figure 4.1: Assembly of the manufacturing simulation of the bowl.

The plate was meshed with explicit axisymmetric linear elements CAX4R with default settings. Mesh size was set as 5 elements through the thickness, which lead to an element size of 0.6 mm. Contact conditions between all parts was set to an estimated friction coefficient $\alpha = 0.2$. The rigid die and holder were applied boundary conditions such that they were fixed in space. The centre of the plate and the punch were set free in the vertical direction and fixed in the other. The velocity of the punch was set to 1 m/s. Material properties of the plate were described in section 3.2 and can be found in appendix A.3.

For the implicit springback simulation, the die, punch, and holder were removed. The final stress and displacement field from the explicit analysis were imported as a predefined field in an initial state. The centreline of the plate was free to move in all directions except horizontally and the bottom left corner of the plate was fixed in space. The boundary condition can be seen in Figure 4.2.

The resulting simulated stresses were then compared with the stresses measured on the bowl. The measurements are done according to EN-SS 15304:2008 with x-ray diffraction where Bragg's law is used to calculate the lattice spacing which is then used to calculate the residual stress. Stress measurements are made on two different bowls before and after heat treatment in the x-direction (radial) and z-direction (tangential) in the coordinate system of Figure 4.2. A comparison was also made between different parameters e.g., velocity and yield stress. A check for the amount of artificial strain energy that was needed in the simulation was also done. The artificial strain energy is the energy created to resist hourglass effect. This was done to verify the explicit simulation. If the artificial strain energy was too high the results in the analysis could be questionable.

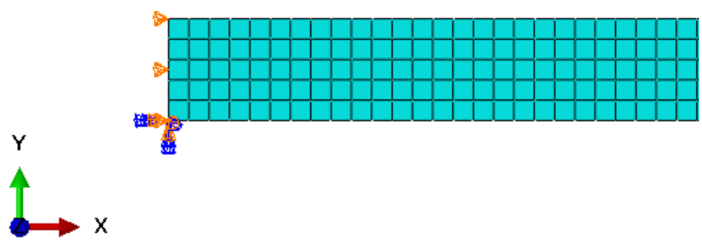

Figure 4.2: Boundary condition for the implicit springback simulation.

4.2 Result

Figure 4.3 and Figure 4.4 display the normal stresses in the x- and z-direction respectively after the explicit bending. The z-direction represents the tangent stress in the same direction in which the residual stresses were measured. To get the same stress direction for the radial stress, coordinate systems in the points of interest need to be applied to capture the stress along the outside of the bowl. This means that the result shown in Figure 4.3 is not the stress field that will be compared to the measured results. In Figure 4.4, it is seen that the stress in the z-direction has its maximum in the bottom of the bowl as well as underneath the contact with the die on the outside of the bowl.

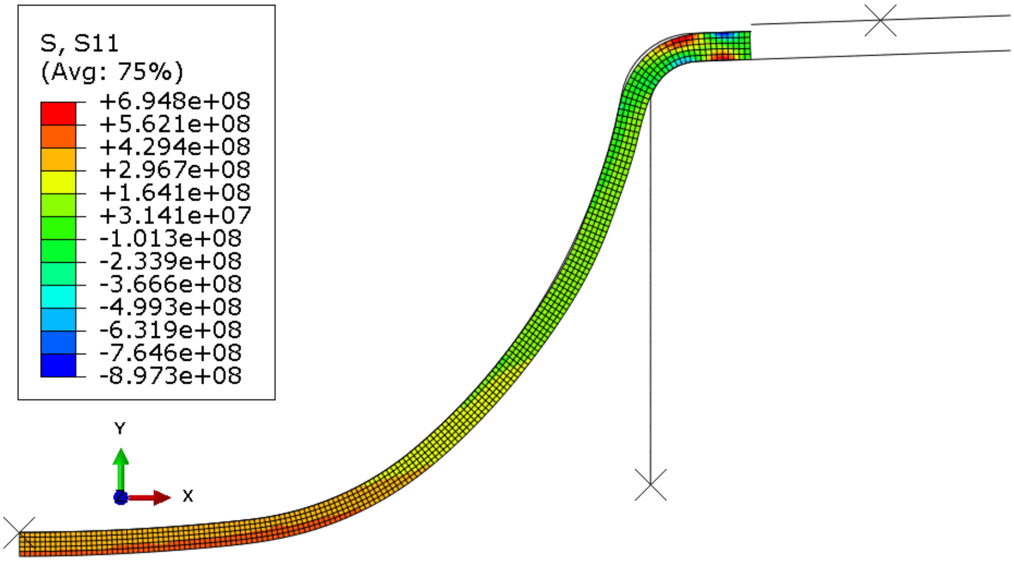

Figure 4.3: Stress result in the x-direction from the explicit simulation.

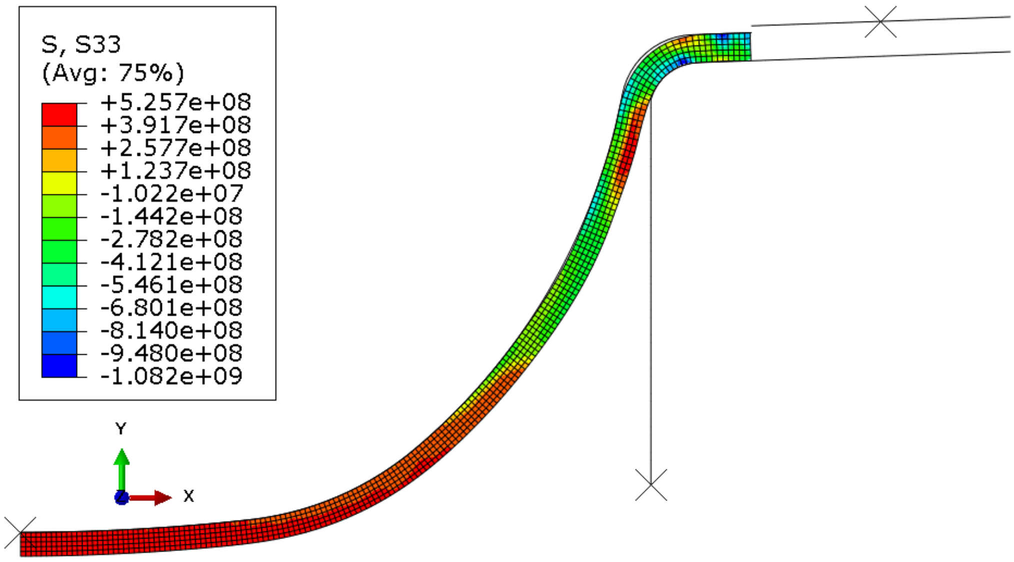

Figure 4.4: Stress result in the z-direction from the explicit simulation.

Displacement caused by the springback effect can be seen in Figure 4.5. The displacements are between 0-40 μm where the largest displacements are in the red area, in the bend at the bottom part of the bowl.

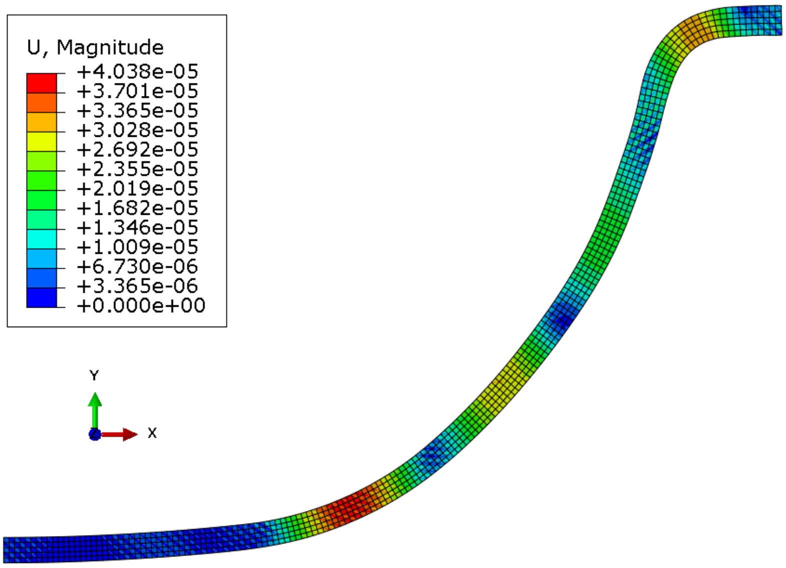

Figure 4.5: Displacement created by the springback effect.

Figure 4.6 shows the stress in the bowl after the implicit springback simulation in the z-direction. The stress magnitude dropped in the entire bowl after the springback. In a comparison before and after the springback simulation, the maximum stress in the z-direction decreased from 526 MPa to 496 MPa. The maximum stress, after the springback, occurs at the bottom of the bowl and underneath the contact with the die on the outside of the bowl. Large compressive stresses can be seen at the inside of the bowl near the contact with the die. One of the contact zones with the punch for the final forming procedure is located in between these two compressive zones.

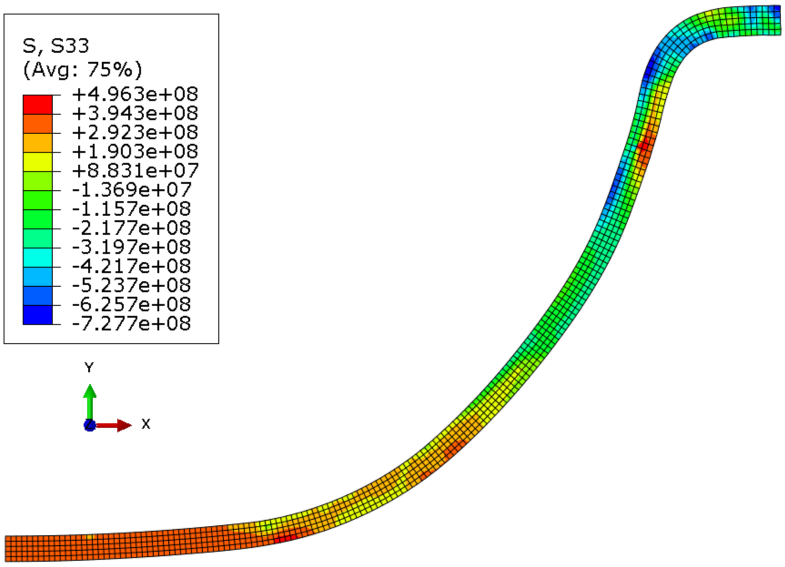

Figure 4.6: Stress field in the z-direction after implicit springback simulation.

To compare the simulation result with the measured results, simulation results were chosen at the same points on the outside of the bowl. The position of the measurements, which was shown in Figure 1.1, were made at 0, 20, 40, 60, 80, 100 mm from the centre of the bowl. Results from the simulated data were taken at the same length from the centre, on the final shape of the bowl. Figure 4.7 displays the position and the coordinate systems in which the results were evaluated. The coordinate systems were applied at the node closest to the measured results. The x-direction of these coordinate systems where in the direction of the closest node to the right.

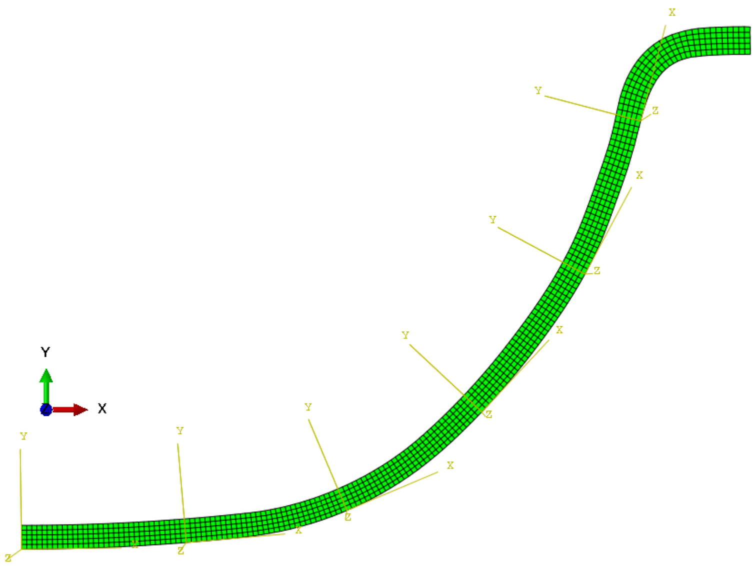

Figure 4.7: Points of interest with radial coordinate systems.

In Figure 4.8 and Figure 4.9 measured residual stress are compared to numerically predicted stresses. In Figure 4.8, the simulated results are corresponding to the measured results in the first two measuring points. The large deviation occurs at 40 mm from the centre. The last three measuring points differ with around 100-150 MPa from the pre-heat treatment results. The points at 60 and 80 mm are however above the stress levels of the results of the post-heat treatment.

Comparing the tangent stress in Figure 4.9, the simulated stress is below the stress levels of the pre-heat treatment stress in all measuring points. The simulated stress is above the post-heat treatment stress levels at all measuring points except for the deviating result at 80 mm. These deviating results at 40 and 80 mm in radial and tangential directions are further discussed in the following section.

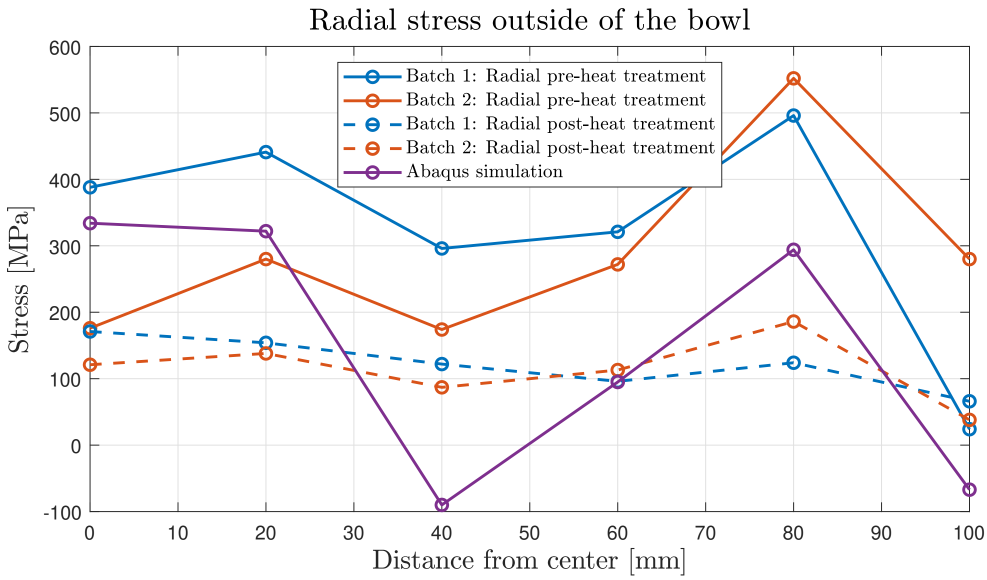

Figure 4.8: Comparison of the measured residual stress and the simulated result in the radial direction.

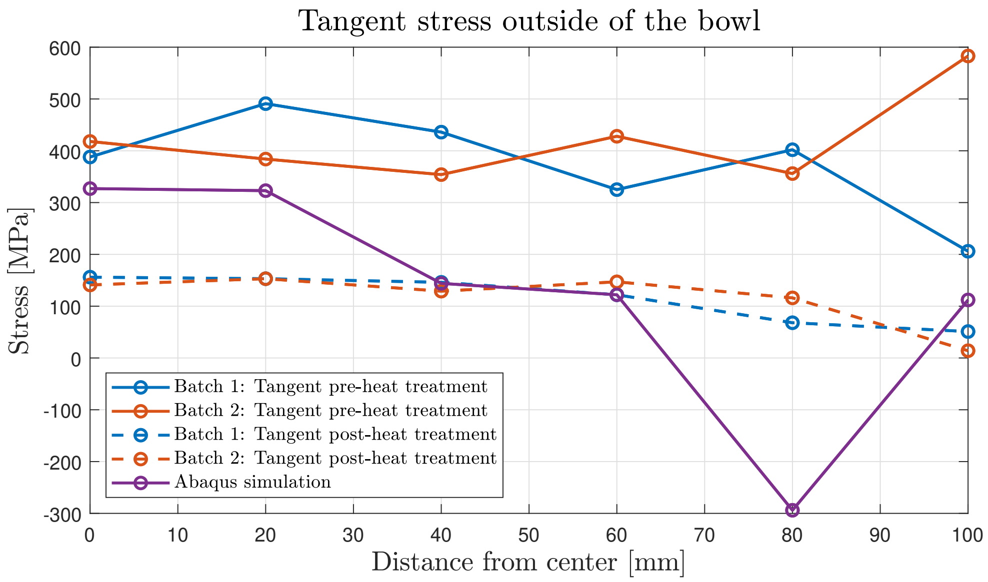

Figure 4.9: Comparison of the measured residual stress and the simulated result in the tangent direction.

Figure 4.10 and Figure 4.11 display magnifications around the 40 and 80 mm points for the x-direction and the z-direction, in the local coordinate system respectively. The red dot points out from where the simulated results are extracted. In Figure 4.10 the stress field goes from tensile on the outside, to tensile stress on the inside, and then back to tensile stress on the outside when traversing in the radial direction. On the opposite side of these tensile stress zones, are compression zones. The result point are taken in the area where the tensile stress is on the inside. Since the surface is curved and the stress is taken in a local coordinate system with origin in the result point (red dot), results in elements with different orientation do not reflect the tangent stress. This result is discussed in section 4.3.

In Figure 4.11, the entire stress field around the result point that sustains compressive stress is displayed. The largest magnitude of compressive stress occurs on the inside above the result point. This is one contact zone where the punch made the final adjustment to the shape of the bowl. The stress displayed in Figure 4.11 is the normal stress in the z-direction, which is the out of plane direction. The result and why it differs from the measured results are discussed in section 4.3.

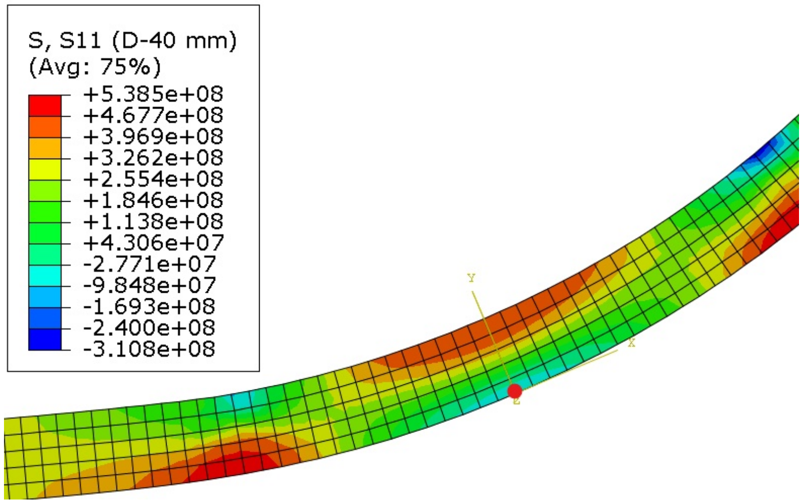

Figure 4.10: Magnification of the stress field in the x-direction in the local coordinate system around the 40 mm point. Element size approximately 0.6 mm.

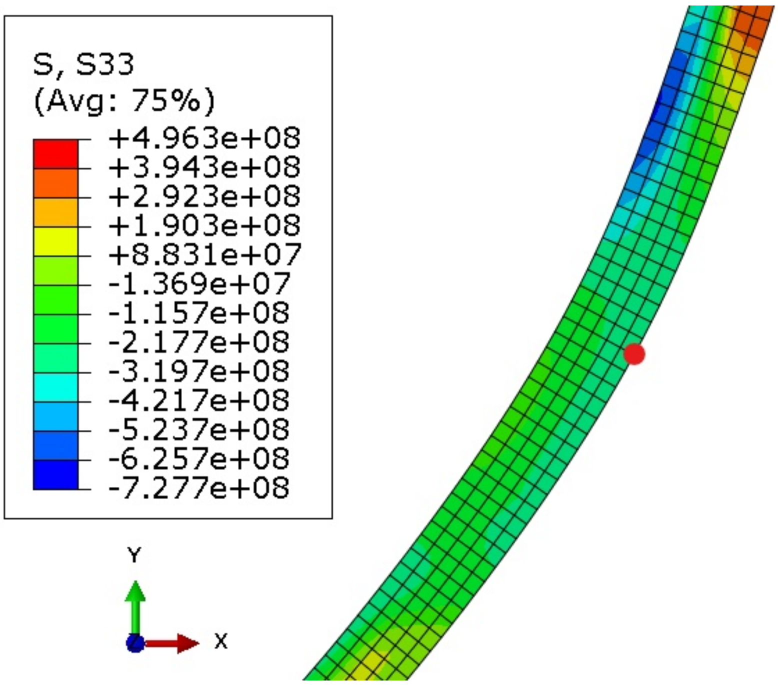

Figure 4.11: Magnification of the stress field in the z-direction around the 80 mm point. Element size approximately 0.6 mm.

Different friction coefficients were tested for the simulation. For friction coefficients higher than 0.5, some elements were drawn out to the point that they lost their integrity and gave unreasonable results. Since the pressing of the plate was adjusted to form the bowl with a friction coefficient $\alpha = 0.2$, a lower fiction coefficient lead to a bowl with a shorter rim. For the case of a lower friction coefficient, the stress field was similar to the stress field with friction coefficient $\alpha = 0.2$.

To examine the impact of the input parameters velocity and yield stress, comparisons of different values were made. The changes were compared with the stress result in the radial direction after the springback. Changes in velocity and yield stress gave insignificant differences in the simulated stress result. The resulting plots of these tests can be seen in appendix A.6. To check if the results were mesh dependent a simulation was made with 7 elements through the thickness. This resulted in a stress field with similar stress magnitudes and appearance. The conclusion was made that 5 elements through the thickness were sufficient.

Analysing the strain energy versus the artificial strain energy (hourglass resistances energy) in the explicit analysis, the artificial energy in the final step of the analysis is 26% of the strain energy. This value is further discussed in section 4.3.

4.3 Discussion

Comparing the results from the simulations with the test data, the largest differences were at two measuring points, one related to stresses in the x-direction and one in the z-direction. The stress field around these points were shown in Figures 4.10 and 4.11. One reason for these differences could be that the simulated manufacturing process is forming the bowl from the inside only. In the real forming process, the punch and die are pressed together to create the shape of the bowl. When this process was tried to be replicated in simulations, the results were nonphysical, and the elements were distorted. Therefore the choice was made to simulate the forming of the bowl only by pressing from the inside.

A resemblance between the two evaluated points is that both have a large compressive zone on the opposite side. These compressive zones coincide with the contact zones between the plate and the punch. During the simulation, the contact between the punch and the plate is not evenly distributed. The contact zones are therefor highly compressed in the final part of the simulation. When studying Figure 4.11, a large compressive zone that starts from the contact affects the stress on the outside of the bowl. In the physical manufacturing of the bowl, a hydroforming technique is used. This allows for an evenly distributed pressure over the entire bowl when pressing the plate into the die. These differences between simulation and manufacturing can be the cause for the different results.

The artificial strain energy versus strain energy ratio is high. The recommended ratio for an explicit analysis is 10%. This implies that the strain to control hourglass deformations is higher than what is optimal. Different settings of hourglass control were tested without improving the artificial strain energy ratio. The reason for this level of artificial energy needs to be further investigated to understand if this affects the stress results.

5

Flex disc simulations

In this chapter, the method and result of the flex disc simulation are presented. The results are discussed in the final section of this chapter.

5.1 Method

The flex disc simulation was done with a midsurface model. It was created by extracting the midsurface from the original CAD model of the flex disc. Since the bending procedure where to be simulated, the midsurface model was flatted out. Due to the rotational symmetric property of the flex disc only one-third of the disc was modelled. Figure 5.1 displays the flattened out midsurface model. Because of the sharp edges created in the symmetry lines, two 5 mm deep edges were added to the model. This was done to avoid unnecessary complications due to meshing, since this part of the model was not of interest for the bending procedure. Modification can be seen in Figure 5.2. The added lines in Figure 5.2 were created to create the mesh of the flex disc, which can be seen in Figure 5.3. The elements were S4R elements with 5 Gauss points through the thickness. Default settings were used for the elements except for the hourglass control which was set to enhanced.

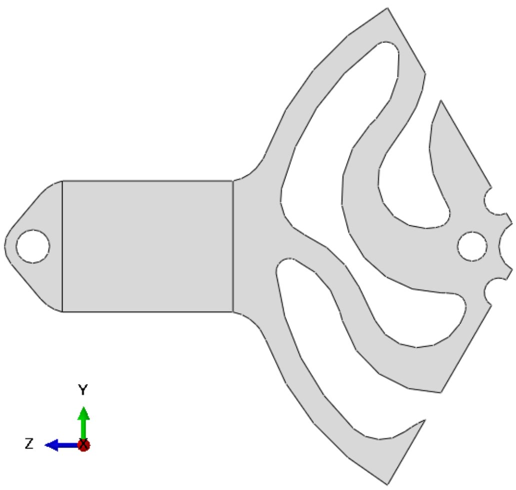

Figure 5.1: Midsurface model of one third of the flattened flex disc.

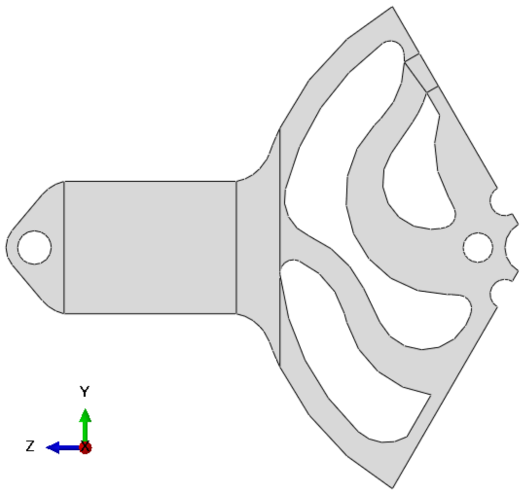

Figure 5.2: Remodeled midsurface model of one third of the flattened flex disc.

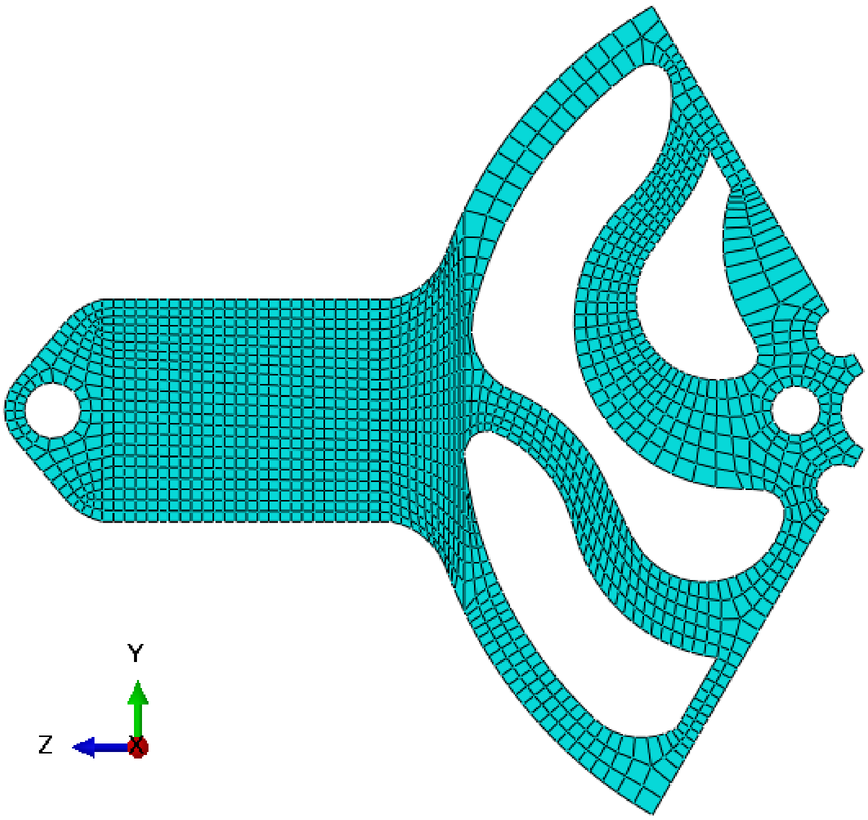

Figure 5.3: Mesh on the midsurface of the flex disc.

The bending procedure was simulated in explicit bending and implicit springback analyses. This was simulated in four steps with a 90-degree bend for each step. Each bending simulation featured a punch and a die. These two parts were modelled as discrete rigid bodies with an element size of 2 mm and a 1 mm mesh size along the curved surfaces. Figure 5.4 shows the setup for the first explicit bending simulation. The right part of the flex disc was set to be fixed in contact with the die as shown in Figure 5.4. The rest of the contact between the die and the flex disc was set to rough, which did not allow any slip between nodes once they were in contact. Contact between the punch and the flex disc was set to frictionless. In the contacts, the rigid bodies were set to be the master surfaces since they were the stiffest. The bending procedure was done by fixing the rigid die in space, fixing the right edge of the rigid punch in all directions except rotation in the y-direction and adding a rotating speed of 2π rad/s in the right edge of the punch in the y-direction. The time of the simulation was then set to 0.25 sec to give a 90-degree bend. The employed material model is presented in section 3.2.

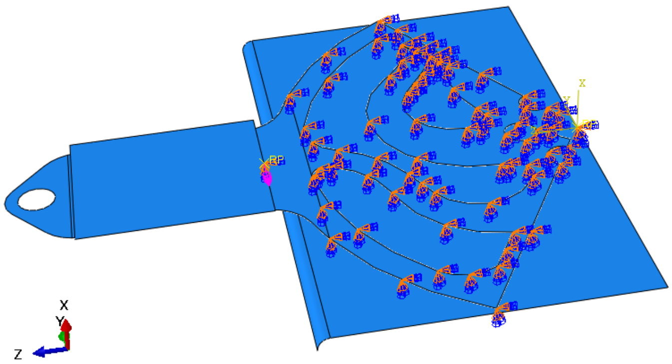

Figure 5.4: Setup for the explicit simulation of the first bend.

Figure 5.5 displays the setup for the implicit springback simulation. The right part of the flex disc was set as fixed in space. Results from the previous explicit simulation were added to the model as a predefined field. This mapped the displacements, the stresses, and the mesh from the explicit simulation onto the flex disc as an initial state. A general static analysis was then done which gave the springback effect with residual stress in the flex disc.

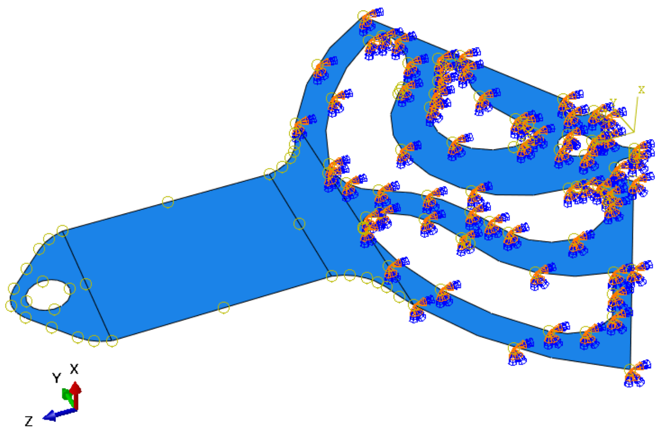

Figure 5.5: Setup for the implicit springback simulation.

Figure 5.6, Figure 5.7 and Figure 5.8 shows the setups for the three next explicit bending simulations respectively. The placements of the die and punch and the time for the simulation had to be adjusted individually for each simulation due to the amount of springback the previous simulation resulted in. To map the predefined fields for the last two steps the import controls normal tolerance had to be adjusted. This was done to avoid mapping issues when two surfaces had their normal position pointing towards each outer. In these simulations, the tolerance was set to 0.5. The resulting stress state was then examined and stresses at the points of interest were extracted and compared to the test result.

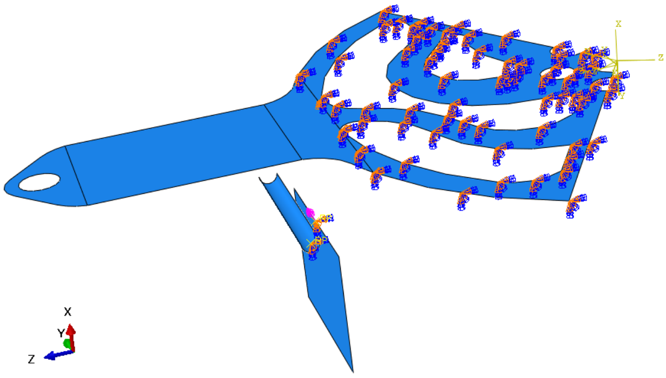

Figure 5.6: Setup for the explicit simulation of the second bend.

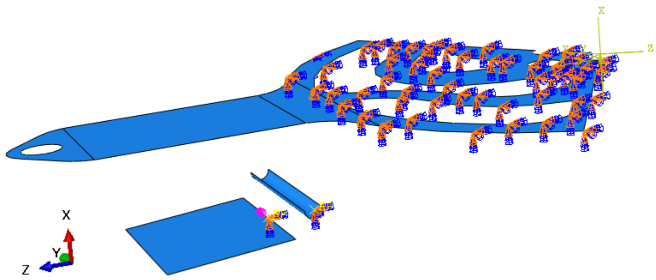

Figure 5.7: Setup for the explicit simulation of the third bend.

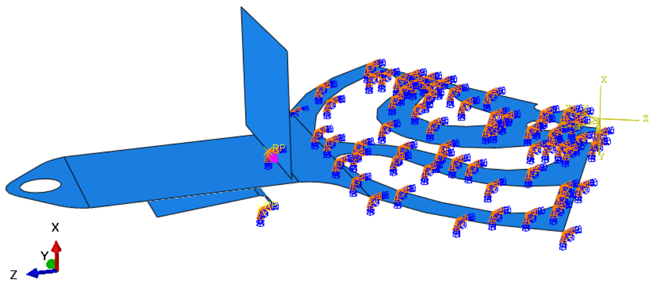

Figure 5.8: Setup for the explicit simulation of the fourth bend.

The welding simulation was done with a symmetry model of a weld nut and a part of the fastener of the flex disc. The simulation was made in two steps, a heat transfer simulation and a general static simulation. The two parts were meshed together to get joint nodes in the contact surface. These nodes were set to be in full contact for both simulations. Figure 5.9 displays the setup for the heat transfer simulation. An increased heat to 1520 ^{o}C for the first 150 ms, which represented the welding time was applied to the joint nodes. Applied heat was then removed and the part was cooled down to room temperature.

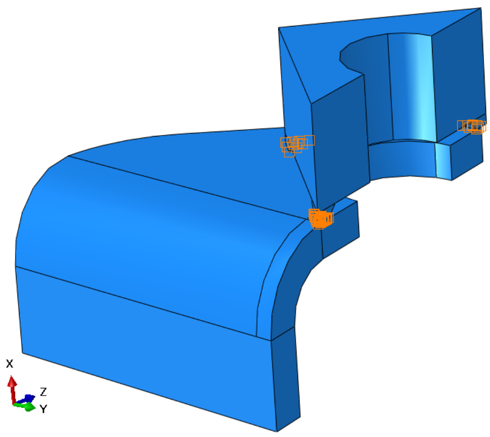

Figure 5.9: Setup for the heating analysis simulating the temperature change in the welding procedure.

The mesh for the weld closest to the 90-degree bend can be seen in Figure 5.10. For the heat transfer simulation, DC3D8 elements were used, which are linear heat transfer bricks. Default settings were used for the element settings. No heat losses were accounted for in the contact between the weld nut and the flex disc. The resulting heating and cooling field were then implemented into the static structural analysis.

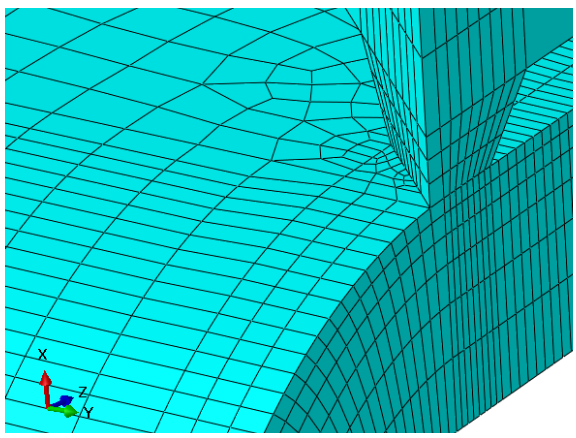

Figure 5.10: Mesh of the weld closest to the 90-degree bend.

For the static structural analysis element type was changed to C3D8R, which are linear brick elements with default settings. The temperature changes were implemented as a predefined field. Figure 5.11 displays the setup for the simulation. The bottom edge of the flex disc was fixed in space, symmetry conditions were implemented in the symmetry surfaces and the bottom part of the flex disc in the horizontal plane was fixed in the x-direction. A pressure load was applied on the top of the weld nut for the first 0.15 seconds of the simulation. This load was simulating the force of 3500 N that was used during the welding procedure. The simulation ran for the same amount of time that the heating and cooling process took. This gave a residual stress field in the parts. The resulting stresses were then examined in the points of interest and added to the stress result in the bending simulation. These results were then compared with the measured test data. The measurements of the flex disc were done in the same manner as for the bowl.

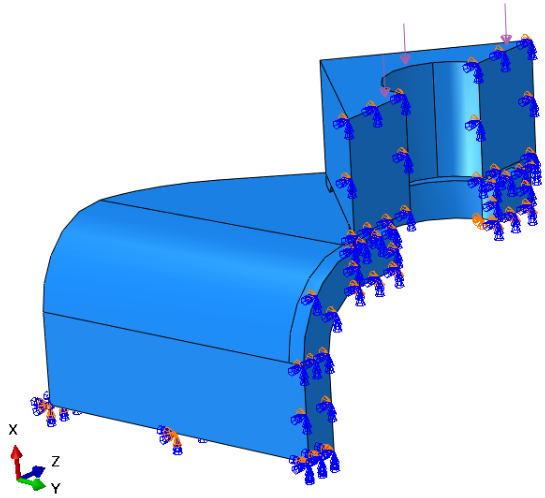

Figure 5.11: Setup for the static analysis simulating stresses during the welding procedure.

To see the impact that the simulated residual stresses have on fatigue life, an oscillating moment was applied to the flex disc in the simulations. This was done on the flex disc with an initial stress state, representing the residual stresses, and on a flex disc without an initial stress state. The moment oscillated between 5 Nm and 95 Nm. Figure 5.12 and Figure 5.13 show the setup for the applied moment for the flex disc with and without initial stress respectively. For the flex disc with an initial stress state, the stress was implemented in the same way as was done in the bending procedure. A cylindrical coordinate system was implemented in the centre of the disc. This was used to set the symmetry boundary condition on the plate. The centre hole of the disc was fixed in space and the bottom of the right part of the flex disc was fixed in the x-direction. The moment was applied as a force in the fastener. The total force was split into four and applied in four nodes, which is displayed in the left part of Figure 5.12. The applied force represented one-third of the force to give a moment of 95 Nm from the centre of the disc. This analysis was done for 95 Nm and 5 Nm. The same procedure was done to the flex disc with no initial stress state. The deformed part was imported from the odb file from the last springback simulation. This gave a part with the same deformation and mesh as the previous simulation. The force were implemented in the same four nodes that was used in the previous simulation.

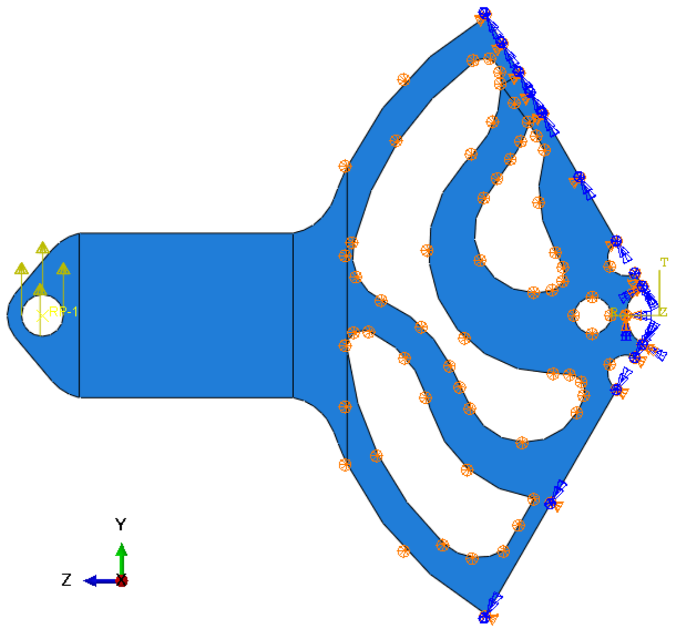

Figure 5.12: Setup for the static analysis with an applied force to simulate the operating moment with an initial stress state.

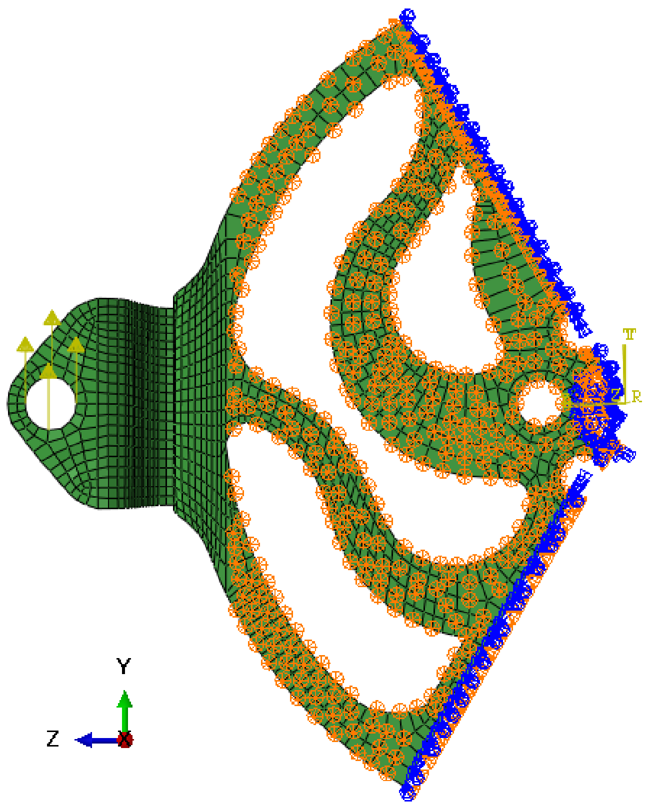

Figure 5.13: Setup for the static analysis with an applied force to simulate the operating moment without an initial stress state.

The final geometry and stress fields were then implemented through odb files into a software called FEMFAT, which is a fatigue life simulation software which is used at Azelio. Parameters inserted into the software was yield stress σ_y=568 MPa, ultimate strength σ_u= 633 MPa and the elongation at rupture A_5 = 35.5 %. Also, the surface roughness was set to roughed which implied a surface roughness of 140 μm. With the geometry, stress field, and these settings a reduced fatigue limit $\sigma_{red,fl}$ and a reduced pulsating fatigue limit $\sigma_{red,flp}$ were given. To ensure that the calculated values were of the right magnitude the Juvinall method of estimating the fatigue limit presented by Dowling et al. [5] was also used. The method is multiplying different parameters to get a reduction factor which is multiplied by the ultimate strength of the material. The reduced fatigue limit and the reduced pulsating fatigue limit were then used to set up a Haigh diagram. Maximum stress amplitude and mean stress were found by subtracting the stresses at the lowest cyclic load from the stresses at the highest cyclic load. This was done in the most critical areas. Finally, the utility and safety factors of the critical points were calculated with the Haigh diagram. For a closer understanding of how these two parameters are calculated, see the literature regarding high cyclic fatigue analysis and safety factor [15].

5.2 Result

The resulting deformation after each explicit bending and implicit springback simulation can be seen in Figure 5.14 to Figure 5.17. The four steps needed to be an extensive bend to adjust for the springback effect. The final shape of the flex disc can be seen in Figure 5.17. Analysing the artificial strain energy versus the strain energy ratio for these four bending simulations, the following results are found for each explicit analysis. First simulation 44%, second simulation 5%, third simulation 12%, and fourth simulation 22% ratio between artificial strain energy and strain energy. These results are further discussed in section 5.3.

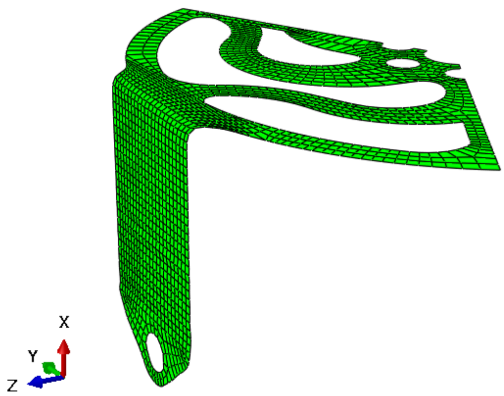

Figure 5.14: Resulting deformation after first explicit bending and implicit springback.

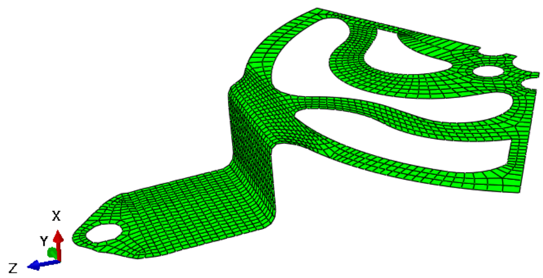

Figure 5.15: Resulting deformation after second explicit bending and implicit springback.

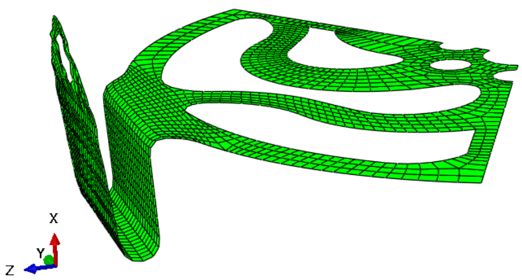

Figure 5.16: Resulting deformation after third explicit bending and implicit springback.

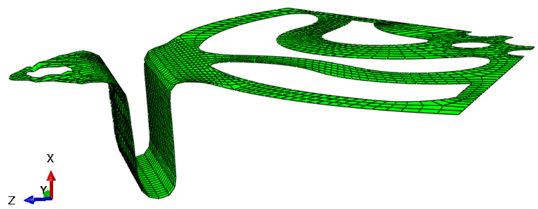

Figure 5.17: Resulting deformation after fourth explicit bending and implicit springback.

Stresses along the outside of the 180-degree bend can be seen in Figure 5.18 to Figure 5.21. Figure 5.18 and Figure 5.19 display the extraction nodes from a right side view with stresses measured in the radial and tangent direction respectively. Figure 5.20 and Figure 5.21 show the same nodes in a left side view with stresses measured in the radial and tangent directions respectively. These stress values are presented in Figure 5.22 along the measured values from the test.

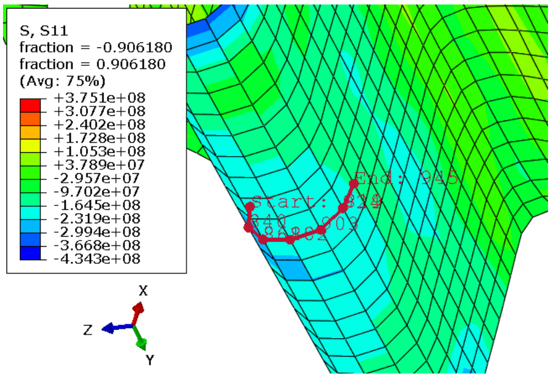

Figure 5.18: Nodes where the radial stress values was extracted at the 180-degree bend, right side.

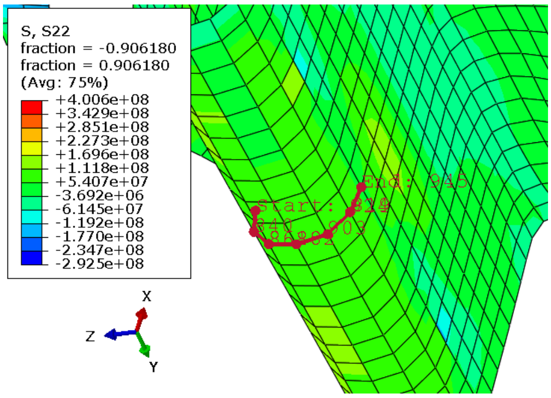

Figure 5.19: Nodes where the tangent stress values was extracted at the 180-degree bend, right side.

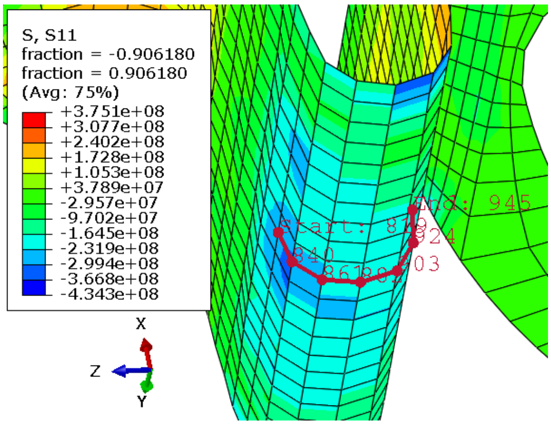

Figure 5.20: Nodes where the radial stress values was extracted at the 180-degree bend, left side.

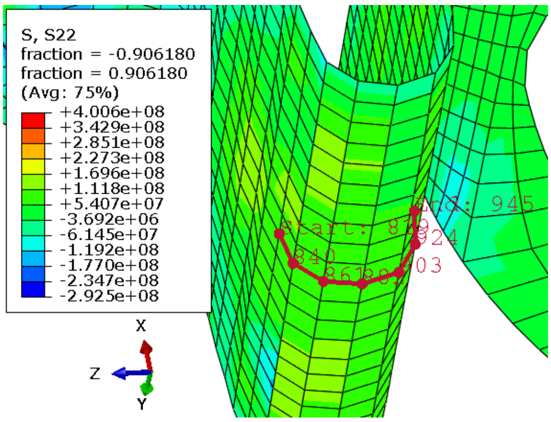

Figure 5.21: Nodes where the tangent stress values was extracted at the 180-degree bend, left side.

By comparing the results, the simulated values are found not to give a compressive stress peak at the middle point, neither in the radial nor in the tangent direction. The simulated results follow a smoother trajectory than the measured results. Stresses in the tangent direction in the simulation are tensile stresses for all seven points while the measured test has two points that are showing tensile stress. Both the simulation and the test results for the radial direction show compressive stress for all measuring points. The average deviation from test data in each point is 110

MPa in the radial direction and 130 MPa in the tangent direction with the largest at point 6 in the radial direction and point 3 in the tangential direction. Plotted values can be seen in Table A.5 in appendix A.8.

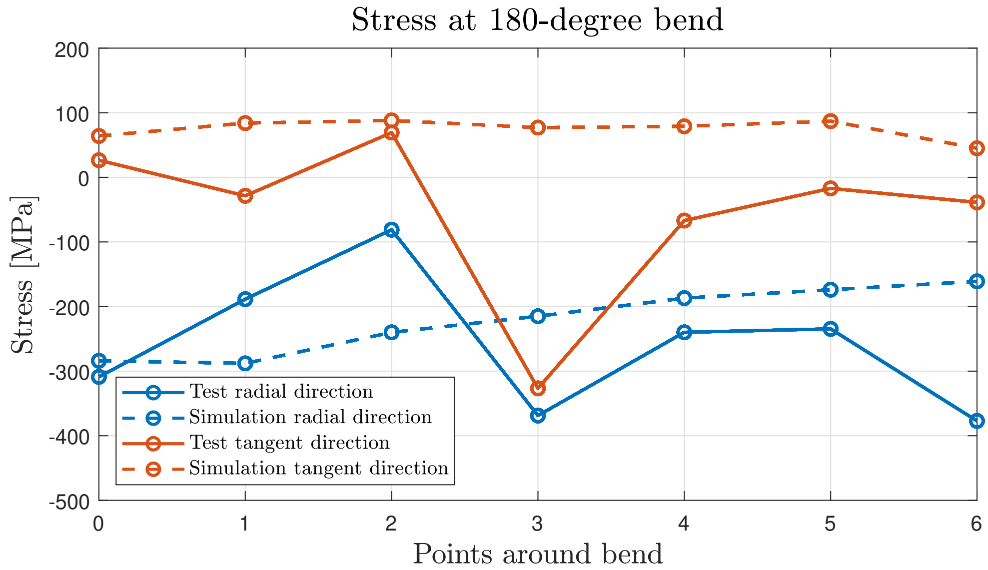

Figure 5.22: Plot comparing test data with simulation results at the 180-degree bend.

Figure 5.23 displays the temperature field at the highest temperature in the weld closest to the bend. The temperature field at each weld does not cross over between the welds and the shape of the weld nugget agrees with the shape discussed in section 3.3. Figure 5.24 and Figure 5.25 show the resulting stress field in front of the weld in radial and tangent direction respectively. Stress results were taken at 1 mm, 3 mm and 5 mm from the weld toe. These results were then added to the results from the bending simulation at the same position.

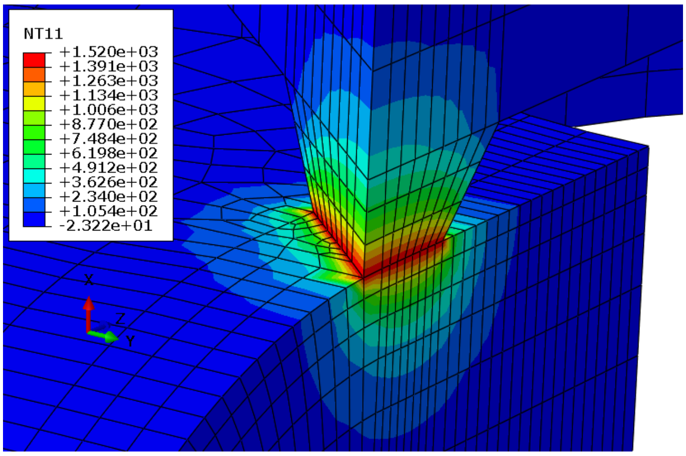

Figure 5.23: Temperature field at weld at maximum temperature.

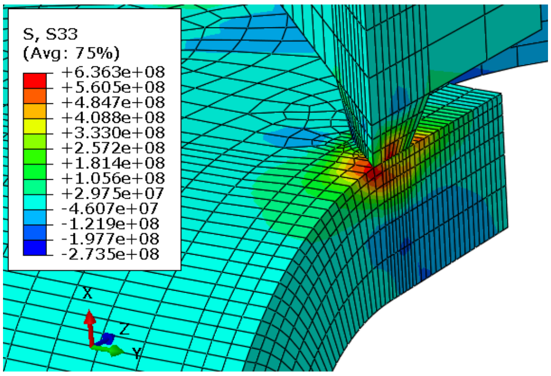

Figure 5.24: Radial stress after welding process.

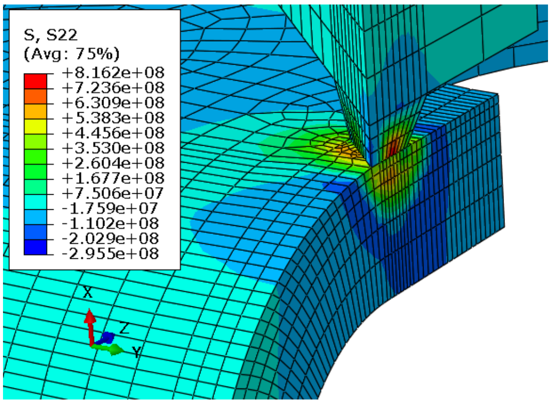

Figure 5.25: Tangent stress after welding process.

Figure 5.26 and Figure 5.27 display the residual stresses at the top of the 90-degree bend in the radial and tangent direction respectively. The highlighted nodes in Figures 5.26 and 5.27 show where the results were taken. Due to the length between the elements the stress values at 1 mm, 3 mm and 5 mm were found through interpolation. The combined results compared with the test data are presented in Figure 5.28 and Figure 5.29.

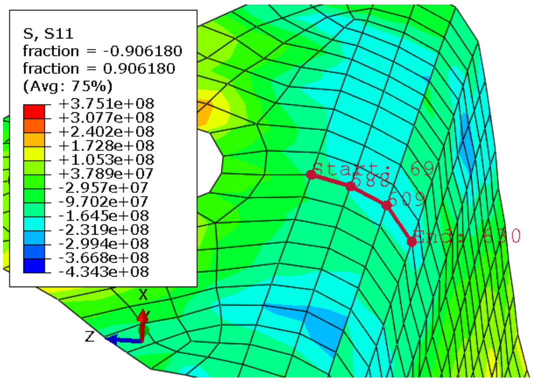

Figure 5.26: Nodes where the radial stress values was extracted at the 90-degree bend.

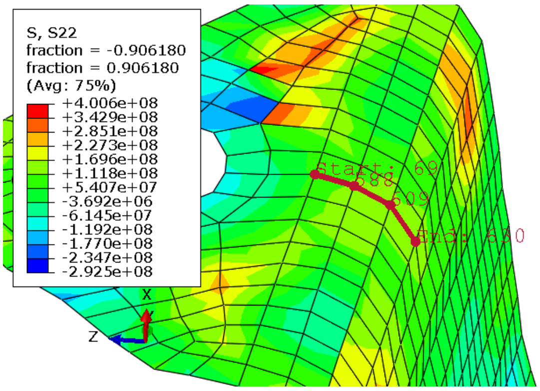

Figure 5.27: Nodes where the tangent stress values was extracted at the 90-degree bend.

Figure 5.28 displays the comparison between test data and the resulting stresses from simulation in the radial direction at the 90-degree bend. Test data are presented in blue and simulation results are presented in orange. The dashed lines represent the results from the weld profile and the solid lines represent results from the radius profile. Combined results from the weld simulation and bending simulation are presented as the simulation weld profile. The result at the radius profile is assumed to be the simulated weld profile result without added stress from the weld simulation. Comparisons between test data and simulation results show that simulation results at the radius profile have similar compressive stresses as found in tests. The result at 1 mm and 5 mm are not as low as the test data shown, but the stress value at 3 mm is at the average of the three test data points at 3 mm distance from the weld toe. Comparing the test data at the weld profile with the simulation, the stress at 1 mm is higher than the tests and the results at 3 mm and 5 mm do not affect the stresses as much as the test data shows. Although the simulations are off by 100-150 MPa at some points, the results show similar development over the bend. The added weld simulation, despite being simplified a lot, showed tensile stress close to the weld toe that faded further away which agrees with the test data.

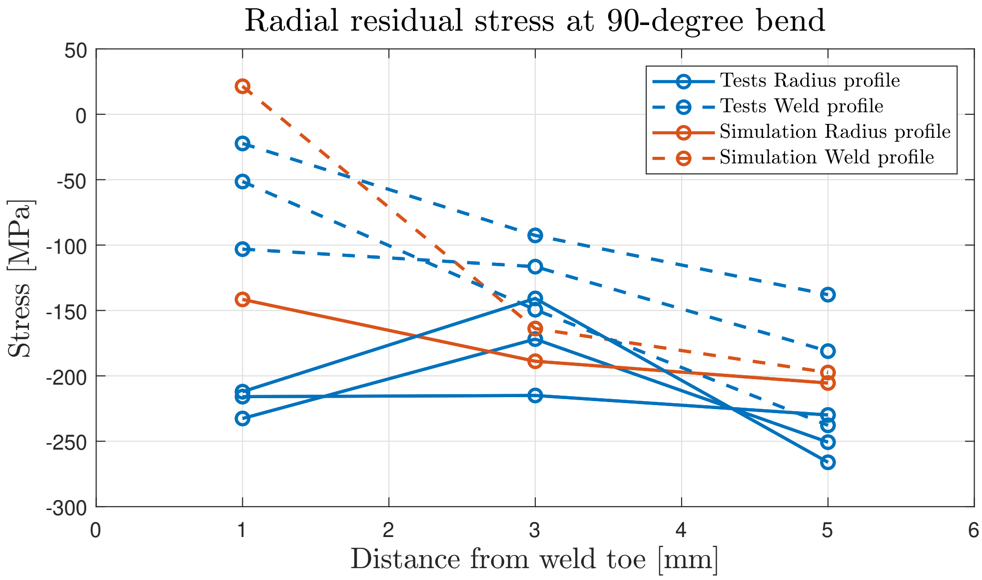

Figure 5.28: Plot comparing test data with the simulated results in the radial direction at the 90-degree bend.

Figure 5.29 shows the comparison between test data and the resulting stresses from simulations in the tangent direction at the 90-degree bend. The results are presented in the same manner as for the stress in the radial direction in Figure 5.28. Since there were only test measurements at 1 mm and 3 mm from the weld toe, the comparisons are only made at these two points. Comparing the simulation result with the test data, the stress at the radius profile is approximately 100 MPa higher than found in the tests. For the weld profile, the compressive stress that was caused by the welding procedure was not of the same magnitude in the simulation as found in the test data. In the tangent direction, the simplified welding simulation does not seem to provide a good representation of the welding process's impact on the residual stress.

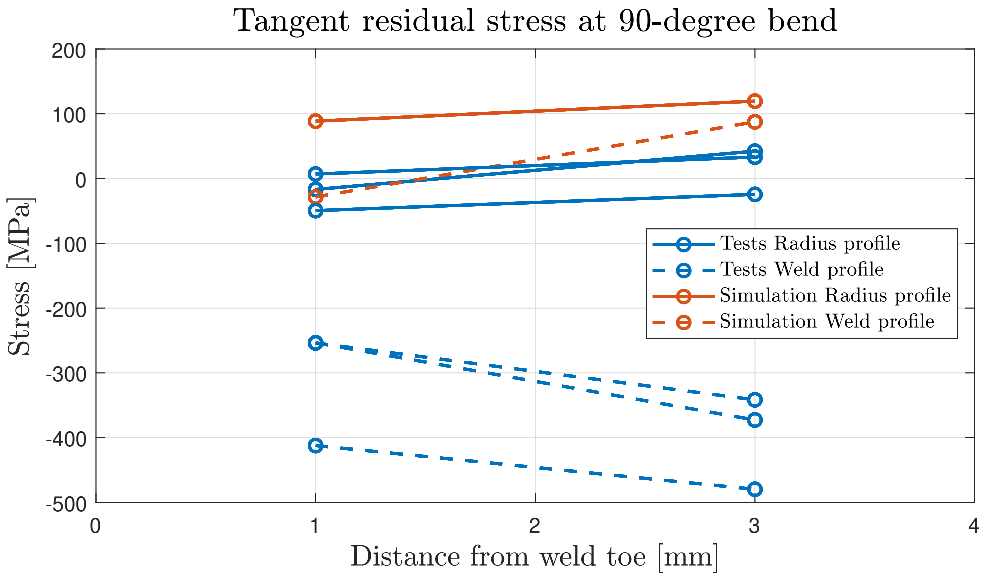

Figure 5.29: Plot comparing test data with the simulated results in the tangent direction at the 90-degree bend.

In Figure 5.30 the critical stress point in maximum principal in-plane stress is presented for the maximum cyclic load case with initial stress. It is located at the top part of the 180-degree bend presented in the figure as element 374. When subtracting the stresses created by the lowest cyclic load, the maximum stress amplitude was found in element 307 and the highest mean stress was found at element 374. These two points are plotted in Figure 5.32 and the exact values are presented in Table 5.1.

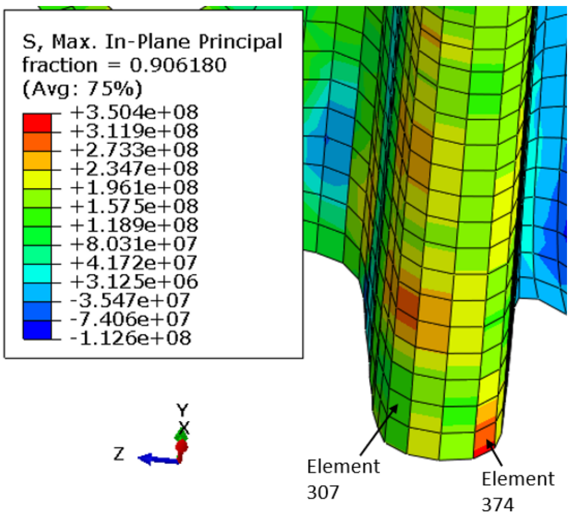

Figure 5.30: Stress concentration after maximum applied force at flex disc with initial stress.

Figure 5.31 displays the critical stress point in maximum principal in-plane stress presented for the maximum cyclic load case without initial stress. It is located at the top part of the 180-degree bend in element 307. Since element 374 are not in the stress concentration zone, the stress concentration seen in Figure 5.30 at this point is residual stress caused by the bending procedure. When subtracting the stress created by the lowest cyclic load, the maximum stress amplitude and the maximum mean stress were found at element 307. This point is plotted in Figure 5.32 and the exact values are presented in Table 5.1.

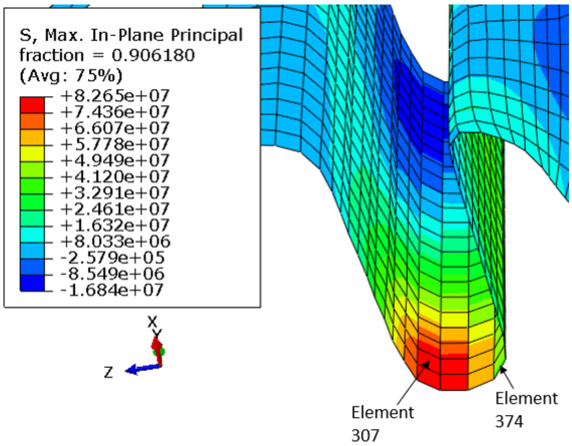

Figure 5.31: Stress concentration after maximum applied force at flex disc without initial stress.

In Figure 5.32 the local Haigh diagram is presented. The reduced fatigue limit $\sigma_{red,fl}$ and the reduced fatigue limit pulsating $\sigma_{red,flp}$ was found through the software FEMFAT, $\sigma_{red,fl} = 275$ MPa and $\sigma_{red,flp} = 235$ MPa . To ensure that the reduced fatigue limit was of the right magnitude, the fatigue limit from FEMFAT was compared with Juvinall's method of estimating fatigue limit. The reduction factors accounted for in the calculation were a bending fatigue limit factor of 0.5 and a surface finish factor of 0.78 which gave an estimation of the fatigue limit of 247 MPa. This comparison shows that the two fatigue limits are of similar magnitude. The calculated utility and the safety factor for fatigue are presented in Table 5.1. According to the safety factors the most critical point is at element 374 at the highest mean stress. Due to the initial stress, the mean stress is higher for element 307 with initial stress than without initial stress. Therefore the safety factor is lower for the simulation with the included residual stress.

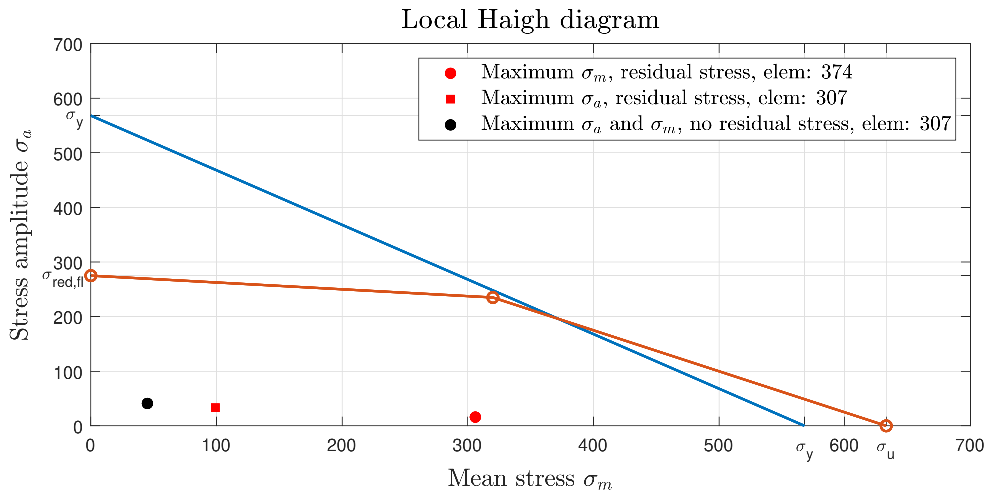

Figure 5.32: Local Haigh diagram displaying maximum stress amplitude and mean stress for the flex disc with and without initial stress state.

Table 5.1: Results plotted in Figure 5.32 and calculated utility and safety factor fracture.

	Element	σ_m [MPa]	σ_a [MPa]	Utility	Safety factor
Residual stress	374	306	16	0.52	1.93
	307	99	33	0.23	4.42
No residual stress	307	45	41	0.17	5.90

5.3 Discussion

During the explicit bending simulation, there was a waviness that developed in the midsurface model. This waviness was found not only where the punch and plate were in contact but also at the end of the fasteners, where the first two bending simulations did not have contact with the flex disc. This waviness grew for each bending simulation and the waviness of the final shape can be seen in Figure 5.33. These waves gave small stresses in various directions. The reason for this waviness was not found during this thesis work. Attempts to reduce the waviness were made. Changing the hourglass control did not reduce the waviness, and neither did taking away reduced integration. To get a larger contact surface, a larger punch was implemented without any reduction in the waviness. When analysing the contact pressure between the punch and the flex disc it was discovered that the pressure was not evenly distributed over the flex disc. The pressure had a spotted pattern in the contact that shifted pattern throughout the bending simulation. The reason for this behaviour needs to be investigated further to understand the simulation result.

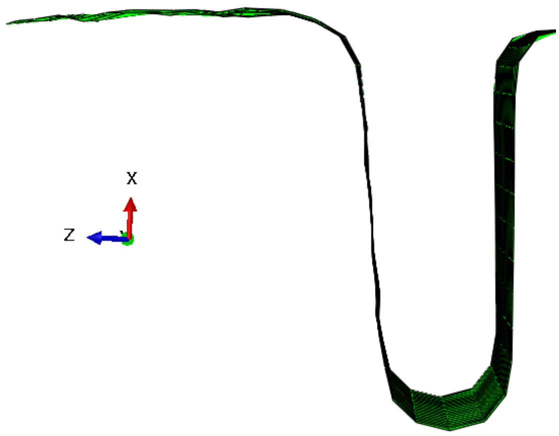

Figure 5.33: Waviness developing in the plate during the explicit bending simulations.

Figure 5.34 displays one nonphysical phenomenon that appears at the fastener due to the waviness discussed earlier. It shows the fasteners after the last springback simulation. In the figure, there are adjacent elements that show maximum tensile stress and maximum compressive stress. This is not physical which makes the other results in this area questionable. This type of phenomenon was only found in the tangent direction at the position shown in Figure 5.34.

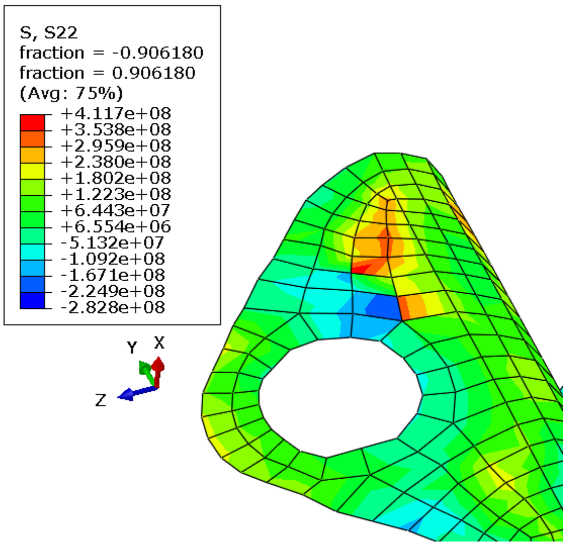

Figure 5.34: Nonphysical phenomena at the fastener.

By analysing the artificial strain energy ratio there seems to be no direct connection between the amount of waviness with the amount of strain energy. The first bending simulation gave 44% artificial strain energy versus strain energy and the second bending simulation gave 5% but there could not be seen a large difference in the amount of waviness that was created in the two simulations. Since the waviness did appear even without reduced integration this could mean that the waviness does not depend on the artificial strain energy ratio. To use this method of simulating residual stresses both the reason for the waviness and why the artificial strain energy is high, need to be investigated and understood to truly trust the simulated results.

The result from the 180-degree bend displayed in Figure 5.22 shows deviating compressive stress in the test data at the middle point of the bend, point 3. This could be due to a clamping mark that could be found on the flex disc. Figure 5.35 displays the bottom of the 180-degree bend where the measurements were made. The clamping mark goes across the measuring point 3. This could be the reason for the deviating results at this point.

Figure 5.35: Clamp mark on the outside of the 180-degree bend.

When analysing the stress amplitude for element 307, the stress amplitude without residual stress has a higher amplitude, 41 MPa, than the same simulations with residual stress, 33 MPa. Since both simulation have the same geometry, load case, and boundary conditions the amplitude should be the same. The reason for this result was not found, but it could be that the nonphysical stress result described earlier deform differently when a force is applied and that gives a different stress result. This, however, is not proven and different simulations are needed to test why the two simulations give different results.

6 Future work

To continue with this method of calculating residual stresses after manufacturing, some results need to be understood better. The first one is to understand why the artificial strain energy versus the strain energy ratio becomes higher in the first bend than in the other three and what could be done to mitigate the artificial strain energy? The second result that needs to be understood is why the waviness occurs. What can be done to take away this result and how much does it impact the comparisons between the simulation results and the measured data?

Once these results are understood, the next step would be to combine the welding simulation with the bending simulation. Adding the residual stress from the bending simulation as an initial state in the welding simulation. Would this give a different result from what was calculated in this report?

7 Conclusion

Residual stresses can be altered through different post-processing methods e.g., shot peening, and heat treatment. Different manufacturing techniques can be used to change the magnitude of the residual stresses. In welding, parameters such as time, temperature and welding pattern can be changed to alter the residual stresses.

Two software was compared in this study, Abaqus and Ansys. They were chosen based on the literature study and accessibility. The simulations were chosen to be done in Abaqus due to better implementations of material models and advantages in transferring results from explicit to implicit analysis.

An explicit bending simulation in combination with an implicit springback simulation gave a residual stress field in the component. This method simulated the springback after bending and gave good stress magnitudes. The welding simulation was a simplified method where a heat transfer simulation was transferred to an implicit static analysis. This was done to simulate the expansion and contraction due to heating and cooling in the welding process. The simulated stress had the expected stress field but not the expected stress magnitude as compared to measured test data. The reason for these differences could be due to contact conditions in the simulation or differences in physical manufacturing and simulated manufacturing. The bending simulations gave more consistent results in comparison with the measured test data than the welding simulation. A better method of simulating the welding procedure needs to be investigated to provide a more accurate residual stress field.

Comparing the fatigue life predictions with and without residual stresses, the residual stresses increased the mean stress in the critical area of the flex disc. This led to a decrease in the safety factor which has an impact on the fatigue prediction. This means that residual stresses need to be taken into account when predicting the fatigue life, either by simulating the residual stresses or by making a conservative assumption and adding a residual stress factor.

Bibliography

[1] **TWI-global**. (January 2022). *What is residual stress?*. https://www.twi-global.com/technical-knowledge/faqs/residual-stress

[2] Zacharia, T., Vitek, J. M., Goldak, J. A., DebRoy, T. A., Rappaz, M., Bhadeshia, H. K. D. H. (1995). **Modeling of fundamental phenomena in welds**. Modelling and Simulation in Materials Science and Engineering, 3(2), 265. IOP Publishing Ltd.

[3] Goldak, J. A., Akhlaghi, M. (2005). **Computational welding mechanics**. Springer Science and Business Media.

[4] Ottosen, N. S., Ristinmaa, M. (2005). **The Mechanics of Constitutive Modeling**, Elsevier Science and Technology.

[5] Dowling, N.E., Kampe, S.L., Kral, M.V. (2020) **Mechanical Behavior of Materials**, *Engineering methods for Deformation, Fracture, and Fatigue* (Fifth edition). Pearson.

[6] Sun J.S., Lee K.H. Lee H.P (2000) **Comparison of implicit and explicit finite element methods for dynamic problems**, *Journal of Materials Processing Technology, Volume 105* pages 110-118.

[7] Prior, A.M.(1994) **Applications of implicit and explicit finite element techniques to metal forming**. *Journal of Materials Processing Technology, Volume 45*, pages 649-656.

[8] Narasimhan, N., Lovell, M.(1999) **Predicting springback in sheet metal forming: an explicit to implicit sequential solution procedure**, *Finite Elements in Analysis and Design, Volume 33*, pages 29-42.

[9] Yetna n'jock, M., Houssem, B., Labergere, C., Saanouni, K., and Zhenming, Y. (2018). **Explicit and Implicit Springback Simulation In Sheet Metal Forming Using Fully Coupled Ductile Damage And Distortional Hardening Model**, AIP Conference Proceedings 1960, 090014.

[10] Yang, D.Y., Jung, D.W., Song, I.S., Yoo, D.J., Lee, J.H.,(1995) **Comparative investigation into implicit, explicit, and iterative implicit/explicit**

schemes for the simulation of sheet-metal forming processes, *Journal of Materials Processing Technology, Volume 50*, pages 39-53.

[11] Weng, C. C., Peköz, T.(1990) **Residual Stresses in Cold-Formed Steel Members**, *Journal of Structural Engineering (ASCE),n. 6, v. 116*, pages 1611-1625.

[12] Zhang, H., Senkara, J. (2011). **Resistance welding: Fundamentals and applications, second edition**. Taylor and Francis Group.

[13] Nielsen, C.V., Zhang, W., Martins, P.A.F., Bay N. (2015) **3D numerical simulation of projection welding of square nuts to sheets**, *Journal of Materials Processing Technology, Volume 215*, pages 171-180.

[14] Josefsson, B.L., Alm, J., McDill, J.M.J (2018) **SIMPLIFIED FEA MODELS IN THE ANALYSIS OF THE REDISTRIBUTION OF BENEFICIAL COMPRESSIVE STRESSES IN WELDS DURING CYCLIC LOADING** *Proceedings of the ASME 37th International Conference on Ocean, Offshore and Arctic Engineering – OMAE, Volume 11B*

[15] Dahlberg, T. (2001) **Teknisk hållfasthetslära**,(Edition 3:19). Studentlitteratur.

A
Appendix

A.1 Drawing: Bending test

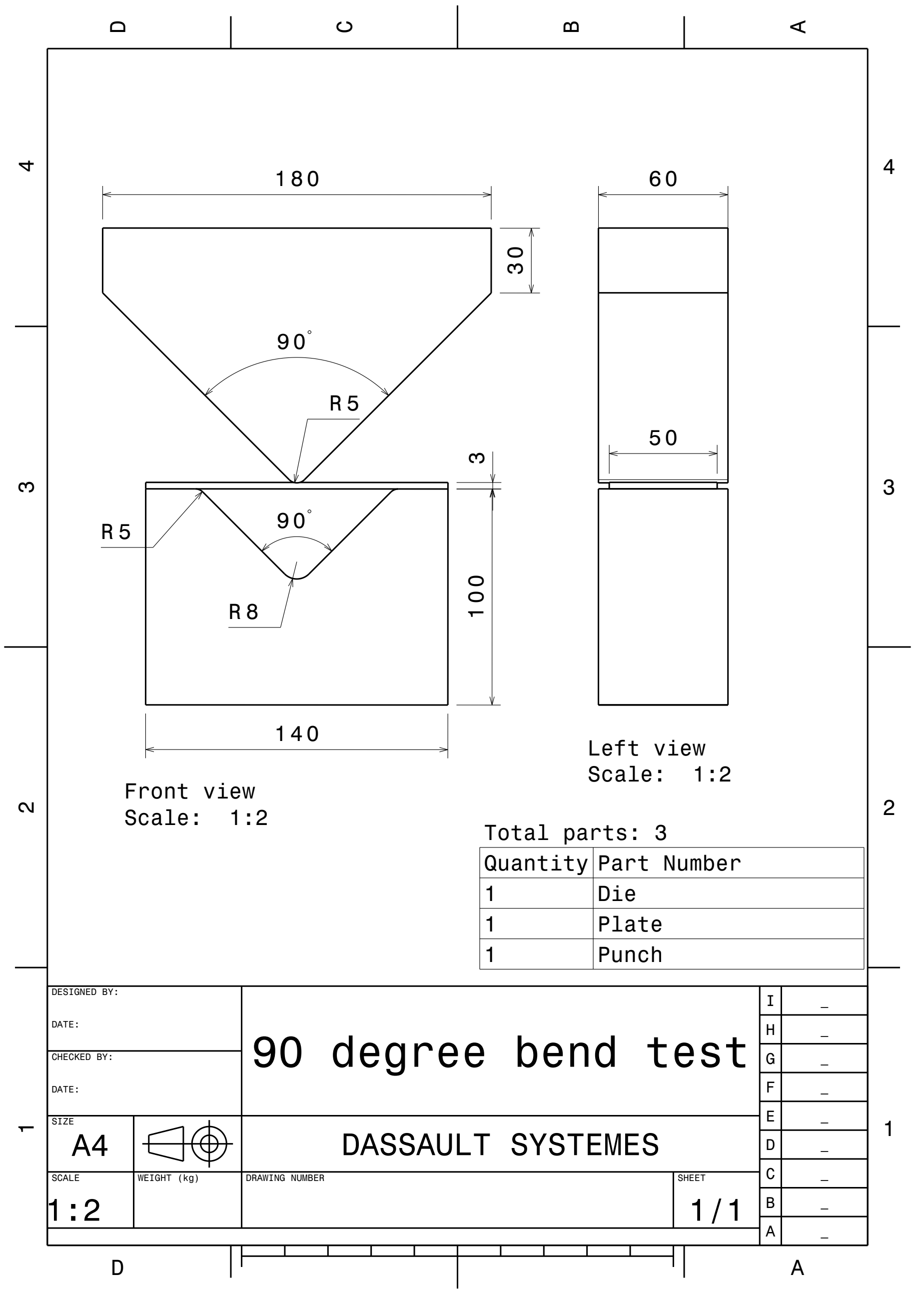

A.2 Drawing: Weld nut test

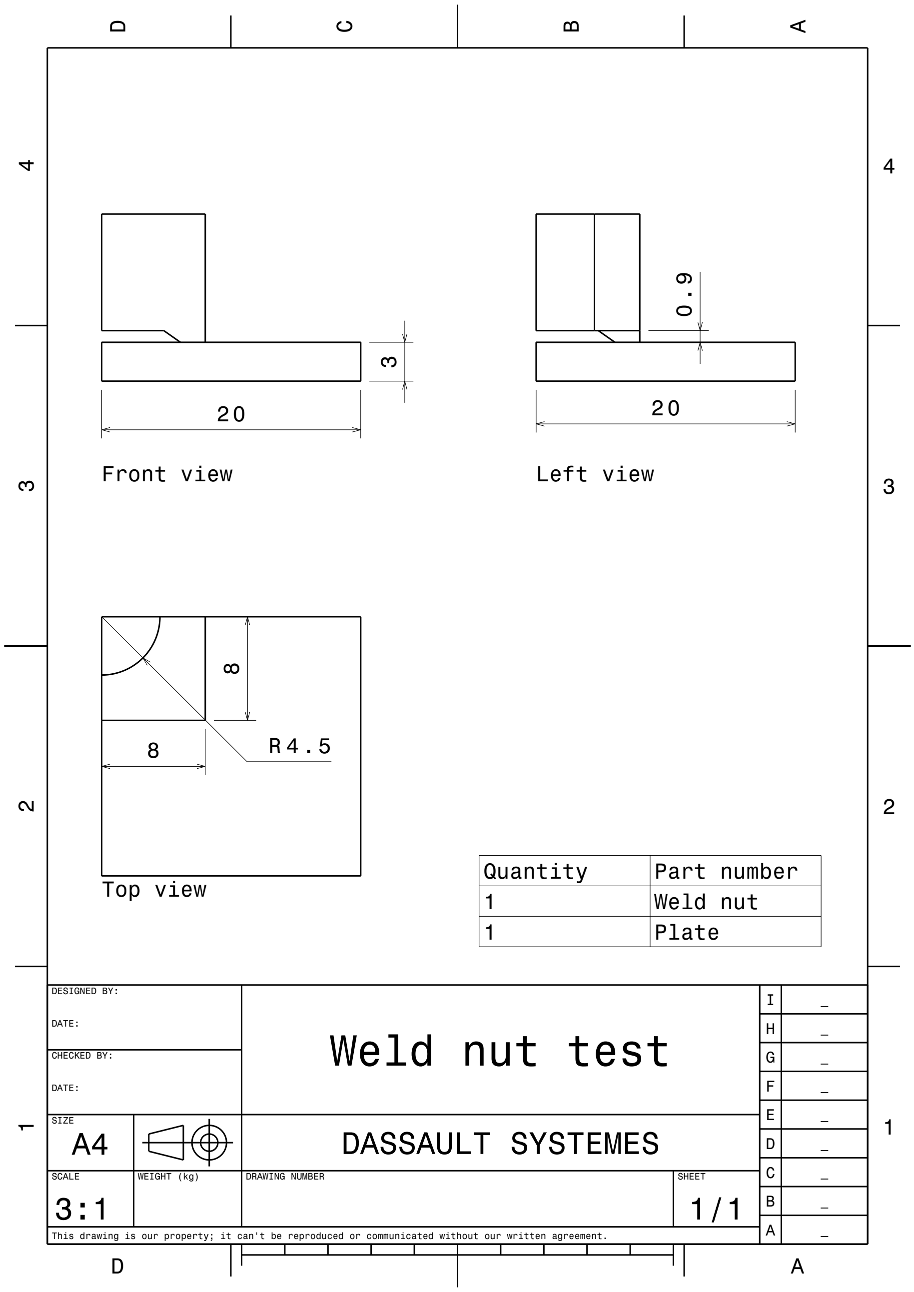

A.3 Material model bowl

Table A.1: Implemented material parameters for the bowl simulation.

Temperature [^oC]	Isotropic elasticity: Young's modulus [GPa]	Isotropic elasticity: Poisson's ratio [-]	Bilinear isotropic hardening: Yield strength [MPa]	Bilinear isotropic hardening: Ultimate stress [MPa]	Bilinear isotropic hardening: Tangent modulus [MPa]	Thermal properties: Thermal conductivity [W/m^oC]	Thermal properties: Specific heat [J/kg^oC]	Thermal properties: Expansion Coefficient [$1/^oC$]
20	200	0.3	350	650	1500*	13	490	$1.65 \cdot 10^{-5}$
100						14	515	$1.65 \cdot 10^{-5}$
200	185	0.33*	232*	514*	1411*	16	540	$1.7 \cdot 10^{-5}$
300			209*	482*	1366*	18	565	$1.7 \cdot 10^{-5}$
400	170	0.37*	179*	430*	1252*	20	580	$1.75 \cdot 10^{-5}$
500			169*	388*	1096*	21	600	$1.8 \cdot 10^{-5}$
600	155	0.4*	123*	283*	801*	23	615	$1.8 \cdot 10^{-5}$
700			71*	149*	390*	24	630	$1.85 \cdot 10^{-5}$
800	135	0.44*	67*	126*	292*	25	645	$1.9 \cdot 10^{-5}$
900			40*	82*	207*	26	655	$1.9 \cdot 10^{-5}$
1000	120	0.48*	27*	52*	127*	28	665	$1.95 \cdot 10^{-5}$

* Approximated value.

A.4 Material model flex disc

Table A.2: Implemented material parameters for the flex disc simulation.

Temperature	Isotropic elasticity		Bilinear isotropic hardening			Thermal properties		
	Young's modulus	Poisson's ratio	Yield strength	Ultimate stress	Tangent modulus	Thermal conductivity	Specific heat	Expansion Coefficient
[^oC]	[GPa]	[-]	[MPa]	[MPa]	[MPa]	[W/m^oC]	[J/kg^oC]	[$1/^oC$]
20	200	0.3	568	633	433*	50*	490*	$1.5{\cdot}10^{-5}$*
100	200*							$1.5{\cdot}10^{-5}$*
200	200*		376*	500*	830*			$1.5{\cdot}10^{-5}$*
300	200*	0.35*						$1.5{\cdot}10^{-5}$*
400	140*	0.37*	291*	419*	849*	40*	625*	$1.5{\cdot}10^{-5}$*
500								$2.4{\cdot}10^{-5}$*
600	70*	0.4*	200*	276*	508*			$2.4{\cdot}10^{-5}$*
700						35*	890*	$2.4{\cdot}10^{-5}$*
800			109*	123*	89*			$2.4{\cdot}10^{-5}$*
900	30*	0.46*					680*	$2.4{\cdot}10^{-5}$*
1000			44*	51*	49*			$2.4{\cdot}10^{-5}$*
1100	20*	0.48*						$2.4{\cdot}10^{-5}$*
1200						30*		$2.4{\cdot}10^{-5}$*
1500						30*		$2.4{\cdot}10^{-5}$*
1520	20*	0.48*				120*	680*	$2.4{\cdot}10^{-5}$*

* Approximated value.

A.5 Material model weld nut

Table A.3: Implemented material parameters for the weld nut simulation.

Temperature [^oC]	Isotropic elasticity: Young's modulus [GPa]	Isotropic elasticity: Poisson's ratio [-]	Bilinear isotropic hardening: Yield strength [MPa]	Bilinear isotropic hardening: Ultimate stress [MPa]	Bilinear isotropic hardening: Tangent modulus [MPa]	Thermal properties: Thermal conductivity [W/m^oC]	Thermal properties: Specific heat [J/kg^oC]	Thermal properties: Expansion Coefficient [$1/^oC$]
20	200	0.3	640	800	1067*	50*	490*	$1.5{\cdot}10^{-5}$*
100	200*							$1.5{\cdot}10^{-5}$*
200	200*		423*	632*	1413*			$1.5{\cdot}10^{-5}$*
300	200*	0.35*						$1.5{\cdot}10^{-5}$*
400	140*	0.37*	328*	529*	1340*	40*	625*	$1.5{\cdot}10^{-5}$*
500								$2.4{\cdot}10^{-5}$*
600	70*	0.4*	225*	348*	820*			$2.4{\cdot}10^{-5}$*
700						35*	890*	$2.4{\cdot}10^{-5}$*
800			123*	155*	213*			$2.4{\cdot}10^{-5}$*
900	30*	0.46*					680*	$2.4{\cdot}10^{-5}$*
1000			49*	65*	107*			$2.4{\cdot}10^{-5}$*
1100	20*	0.48*						$2.4{\cdot}10^{-5}$*
1200						30*		$2.4{\cdot}10^{-5}$*
1500						30*		$2.4{\cdot}10^{-5}$*
1520	20*	0.48*				120*	680*	$2.4{\cdot}10^{-5}$*

* Approximated value.

A.6 Comparison of radial stress of different velocities and yield stresses for the bowl.

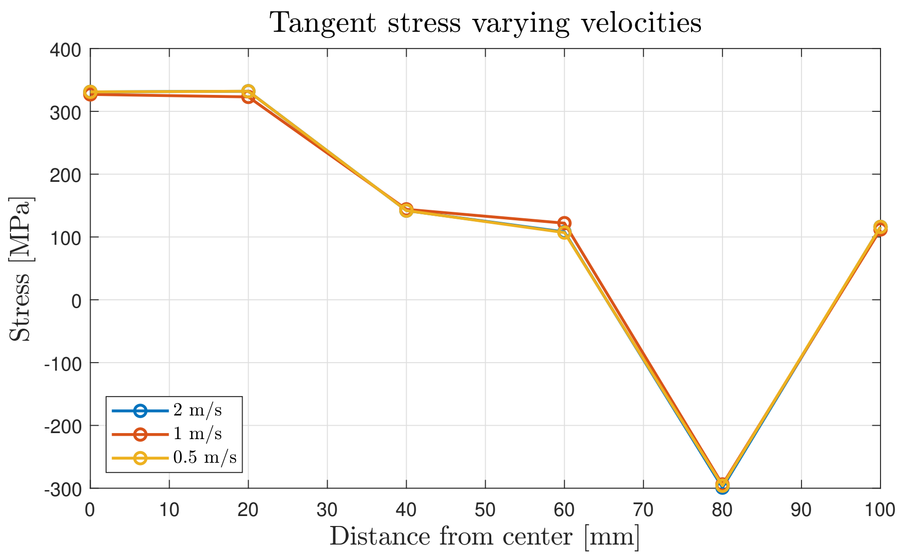

Figure A.1: Comparison of different velocities impact on the radial stress after the springback.

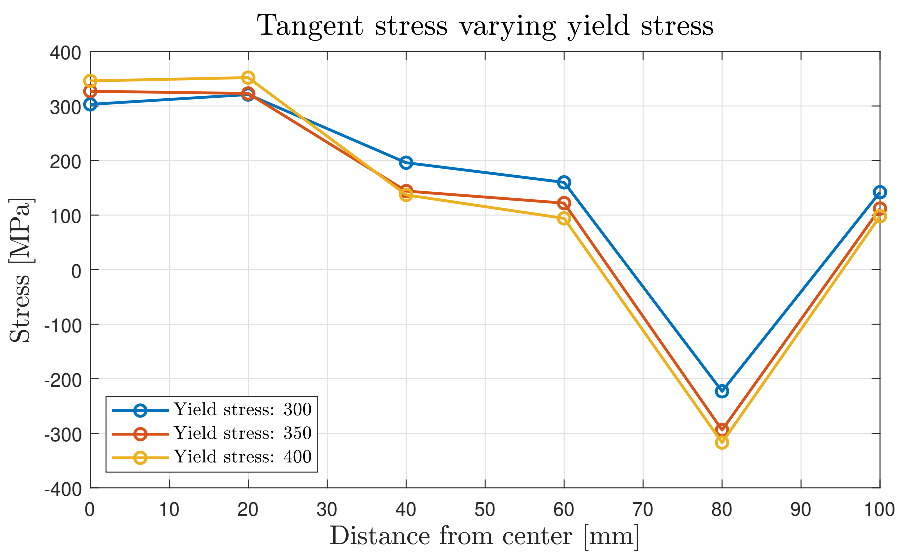

Figure A.2: Comparison of different yield stresses impact on the radial stress after the springback.

A.7 Residual stress values at the 90 degree bend.

Table A.4: Residual stress values plotted in Figure 5.28 and Figure 5.29.

	Position from weld toe [mm]	Position 1		Position 2		Position 3		Simulation	
		Radius profile [MPa]	Welded profile [MPa]	Radius profile [MPa]	Welded profile [MPa]	Radius profile [MPa]	Welded profile [MPa]	Radius profile [MPa]	Welded profile [MPa]
Radial	1	-233	-22	-212	-103	-216	-51	-142	21
	3	-172	-93	-141	-117	-215	-149	-189	-164
	5	-251	-138	-266	-181	-230	-238	-205	-197
Tangent	1	-17	-254	-50	-412	7	-254	89	-28
	3	42	-373	-24	-480	33	-342	120	88

A.8 Residual stress values at the 180 degree bend.

Table A.5: Residual stress values plotted in Figure 5.22.

Position	Test		Simulation	
	Radial [MPa]	Tangent [MPa]	Radial [MPa]	Tangent [MPa]
0	-309	27	-284	64
1	-189	-29	-288	84
2	-81	69	-240	88
3	-369	-326	-215	77
4	-240	-67	-187	79
5	-235	-17	-174	87
6	-377	-39	-161	45

DEPARTMENT OF MECHANICS AND MARITIME SCIENCES
CHALMERS UNIVERSITY OF TECHNOLOGY
Gothenburg, Sweden 2022
www.chalmers.se

CHALMERS
UNIVERSITY OF TECHNOLOGY